APPENDIX A – NUMERICAL MODELLING AND PILLAR/PANEL STABILITY ASSESSMENT

A.1 INTRODUCTION

As part of the Collingwood Park Subsidence Assessment project, numerical modelling was undertaken to assist in the evaluation of backfilling strategies focussed on reducing potential pillar and panel instability. Backfilling of mine roadways surrounding pillars is proposed for the purpose of increasing both immediate pillar strength and reducing the rate of pillar strength degradation from pillar spalling and roadway instability. Backfilled roadways would be expected to reduce surface subsidence, tilt and strains in the unlikely event that pillar failure was to occur after remediation by backfill.

Subsequent to numerical studies, calibrated empirical, or semi-analytical, assessment of every pillar of Westfalen No. 3 colliery was undertaken for the purpose of identifying regions of potential instability.

Towards these objectives the following tasks have been undertaken.

- Literature review of reports on Collingwood Park subsidence events and coal pillar strength and stress calculations by empirical, analytical and numerical methods. Review of the strength based Factor of Safety (FoS) method for pillar design.
- Literature review of backfill properties.
- Calibrating material parameters in numerical models by comparison with the analytical coal pillar strength formula.
- Assessing size, shape and post failure strength parameters and characteristics of coal pillars of dimensions typical of Westfalen No. 3 Colliery.
- Assessing the effectiveness of backfilling roadways surrounding a single square pillar.
- Development of a full three dimensional (3D) numerical model of the Duncan St area comprising 46 pillars and pillar and panel stability assessment for various pillar heights.
- Assessment of various backfill options on pillar stability, surface subsidence, tilt and strain for the 3D Duncan St model.
- Development of a full three-dimensional model of the region to the north east of Duncan St comprising 76 pillars.
- Estimating the strength difference between pillar panels west and east of the Waterline fault from the two 3D models.

Outputs and outcomes from the modelling study include the following.

- An understanding of pre and post-peak strength and shape effects for pillars with typical dimensions of pillars in the Duncan St area.

- An understanding of the pillar strength increase, when surrounding roadways are filled by cohesive and non-cohesive backfill to various heights.
- Understanding of pillar and panel FoS increase from backfill.
- A full 3D model of 46 pillars in the Duncan St area and surface subsidence prediction at nominal 6m mining height and 9m mining height benchmarked with monitoring data.
- Estimates of lateral extent of stress abutment.
- Comparative strength assessment of the two panel layouts west and east of Waterline fault.

A.2 LITERATURE REVIEW ON PILLAR STRENGTH

A.2.1 Pillar strength formula

Several empirical formulas have been developed to calculate mine pillar strength based on experimental field data in the form of a single equation; where pillar strength (S) is equal to an empirical constant (A) times pillar width (w) to a constant power (α) divided by pillar height (h) to a constant power (β), i.e. $S = A * w^{\alpha} * h^{\beta}$.

The empirical equation developed by Salamon & Munro [Salamon 1967, Salamon 1998] (in SI units) has been widely used in South Africa and Australia since its development in 1967:

$$\text{Pillar strength} = 7.2\, w^{0.46} / h^{0.66} \quad (1)$$

where the constant A = 7.2, α = 0.46 and β = 0.66, and

w = pillar width;

h = mining height.

The coal pillar strength equation developed by UNSW, from a database of Australian coal pillars in 1996 [Galvin, 1999] uses different constants given by:

$$\text{Pillar strength} = 8.60\, w^{0.51} / h^{0.84} \quad (2)$$

Coal pillar strength estimated from the combined databases of South African and Australian coal pillars in 1999 [Galvin, 1999] has the following form:

$$\text{Pillar strength} = 6.88\, w^{0.50} / h^{0.70} \quad (3)$$

Interestingly, all the above formulas, Equations (1), (2) and (3), give very similar results, although they are derived for pillars from two different continents with generally different geological conditions and settings [Mark, 1999, Galvin, 1999].

An observation from this is that above a width-to-height ratio of two geometric parameters influence pillar strength rather than the pillar material, below two Galvin

[Galvin, 2006] reports that geological properties of the pillar dominate the overall pillar strength.

A.2.2 Pillar effective width

Wagner [Wagner, 1974] invoked the concept of hydraulic radius to define the effective width w_e as [Wagner, 1980]:

$$w_e = 4 A_p / C_p \quad (4)$$

where

A_p = cross sectional area of the pillar (w^2 for a square pillar)

C_p = cross sectional circumference of the pillar (4w for a square pillar)

and which becomes identical to w for square pillars.

To account for parallelepiped pillars of widths w_1 and w_2 and internal acute angle θ UNSW [Galvin 1999] has expressed the effective width by:

$$w_e = w_m \ \Theta \quad (5)$$

where

$$w_m = w_1 \sin \theta \quad (6)$$

and

$$\Theta = 2 w_2 / (w_1 + w_2) \quad (7)$$

A.2.3 Pillar load

Pillar axial stress can be estimated by [Salamon, 1967, Salamon, 1974]:

$$\text{Pillar stress} = \rho g H / (1 - e) \quad (8)$$

where H is depth of cover, e is the area extraction ratio, which is theoretically between zero (no extraction) and one (100% extraction). To keep consistency with the original parameters of equation (1), gravity and average overburden density are defined as:

$g = 10 \text{ m / sec}^2$

$\rho = 2488 \text{ kg / m}^3$

Using tributary area theory, the original work of Salamon and Munro calculates the loading share of a square pillar of width w, bord width B and depth of mining H as

$$\text{Pillar stress} = \rho g H (1 - e) = \rho g H [(w + B)/w]^2 \quad (9)$$

Assumed in equation (9) is that the stress is fully contained on the pillars that are uniform in size with constant bord width [Salamon 1974, Zipf 2001], which is a conservative assumption [Wagner 1980], and is acceptable if the panel width to depth ratio exceeds unity [Roberts 2002].

One of the outcomes of the present Collingwood Park investigation is the development of a method of estimating pillar loads, where the conditions for tributary area theory cannot be satisfied, as is the case at Westfalen No. 3 colliery in the western branch. This stress estimation method is termed “Pressure Arch theory” (PAt) [Poulsen 2010].

A.2.4 Pressure Arch Theory

When conditions for tributary area theory are not satisfied due to an irregular pillar layout or variable overburden cover an alternative approach to estimate pillar stress is PAt. The main components of PAt are:

- Load is uniquely estimated for every pillar.
- Depth-of-cover (*H* in equation (8)) is calculated at the pillar centroid.
- Extraction ratio ρ in equation (8) is calculated locally, within a zone-of-influence defined by the depth dependent Load Transfer Distance [Abel 1988].

It is important to note that PAt converges to the equivalent tributary area theory (TAt) value when the conditions for TAt are satisfied, Figure A-2.

Zone of Influence

The Zone-of-Influence (ZI) used in PAt is based on the Load Transfer Distance (LTD) defined by Abel [Abel 1988] as the maximum distance any load can be laterally transferred and is determined by measuring the maximum distance that any effect of mining can be detected. Monitoring results from mining in sedimentary strata are displayed in Figure A-1 and the LTD defined as:

$$LTD = -1e\text{-}4\ H^2 + 0.2701\ H \qquad (10)$$

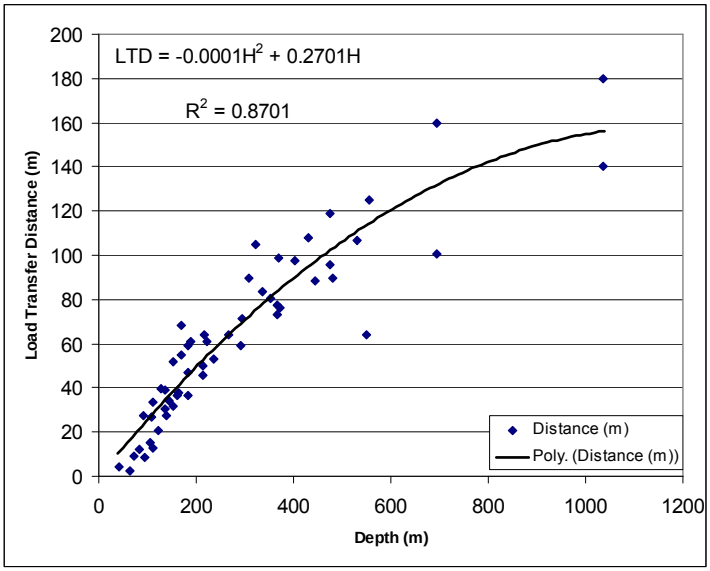

Figure A-1 Load transfer distance with depth for sedimentary strata. (after Abel, 1988)

Pillars within the LTD of each other will be able to interact and shed load. Typically a stiffer pillar, generally of greater width to height ratio such as a barrier pillar, will carry a greater proportion of the load than smaller production pillars within its zone of influence. A pillar of effective width w_e has a lateral zone of influence measured from the pillar centroid of:

$$ZI = 2 * LTD + w_e / 2 \quad (11)$$

ZI in equation (11) is then the radius of a circular influence zone centred on the pillar for which stress is estimated. The extraction ratio in this influence region ρ is then used to estimate pillar stress with equation (8) [Poulsen 2010].

Comparison with numerical models and tributary area theory

Comparison of pillar stress calculated by PAt and numerical models is made in [Poulsen 2010] and in the numerical models constructed after both the 1988 and 2008 subsidence events at Collingwood Park.

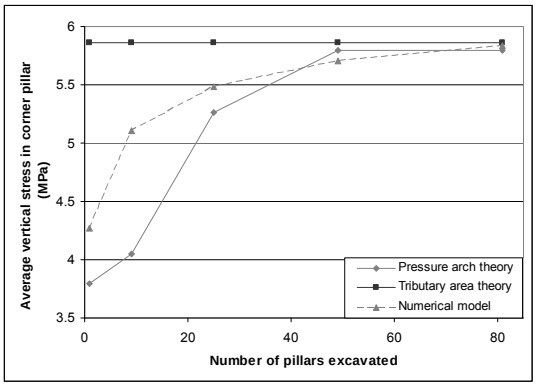

Figure A-2 Stress in central pillar calculated by tributary area and pressure arch theories compared with an elastic numerical model.

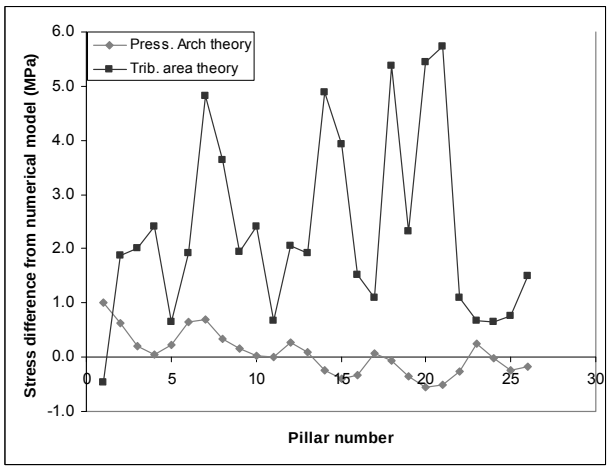

Figure A-3 Stress difference from elastic numerical model for pillar stress estimated by pressure arch and tributary area theories. Average absolute stress difference for pillar stress estimated with pressure arch theory is 0.30 MPa and with tributary area theory is 2.37 MPa.

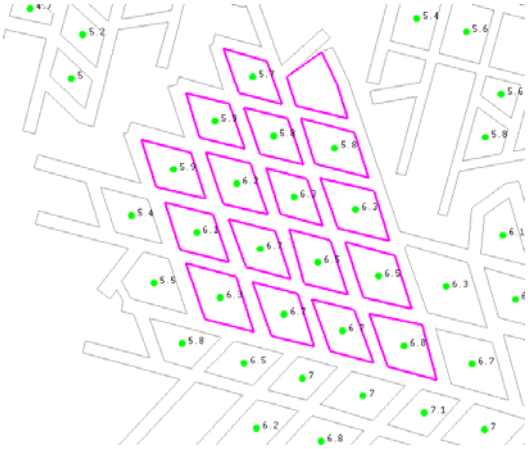

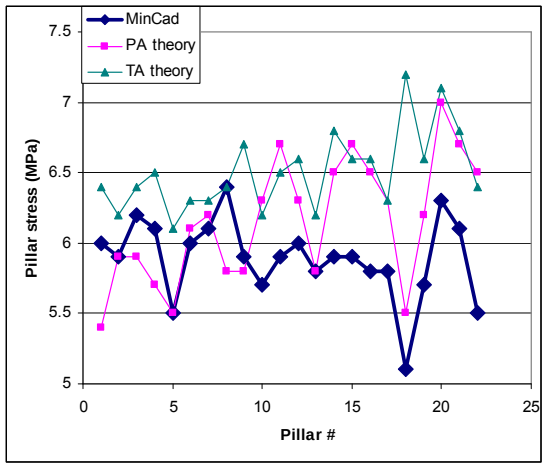

Figure A-4 pillar stresses predicted by pressure arch theory (left) and stresses predicted by pressure arch theory, tributary area theory and MinCad model (right). Average absolute percentage variation from modelling results is 7.5% PA theory and 10.8% TA theory.

After the 1988 subsidence event at Collingwood Park a numerical model was constructed with the code MINCAD and reported in [Wardel 1989]. Stresses predicted by this numerical model, PAt and TAt are made in Figure A-4.

Comparison with Duncan St FLAC3D model constructed for this project is made in Figure A-5.

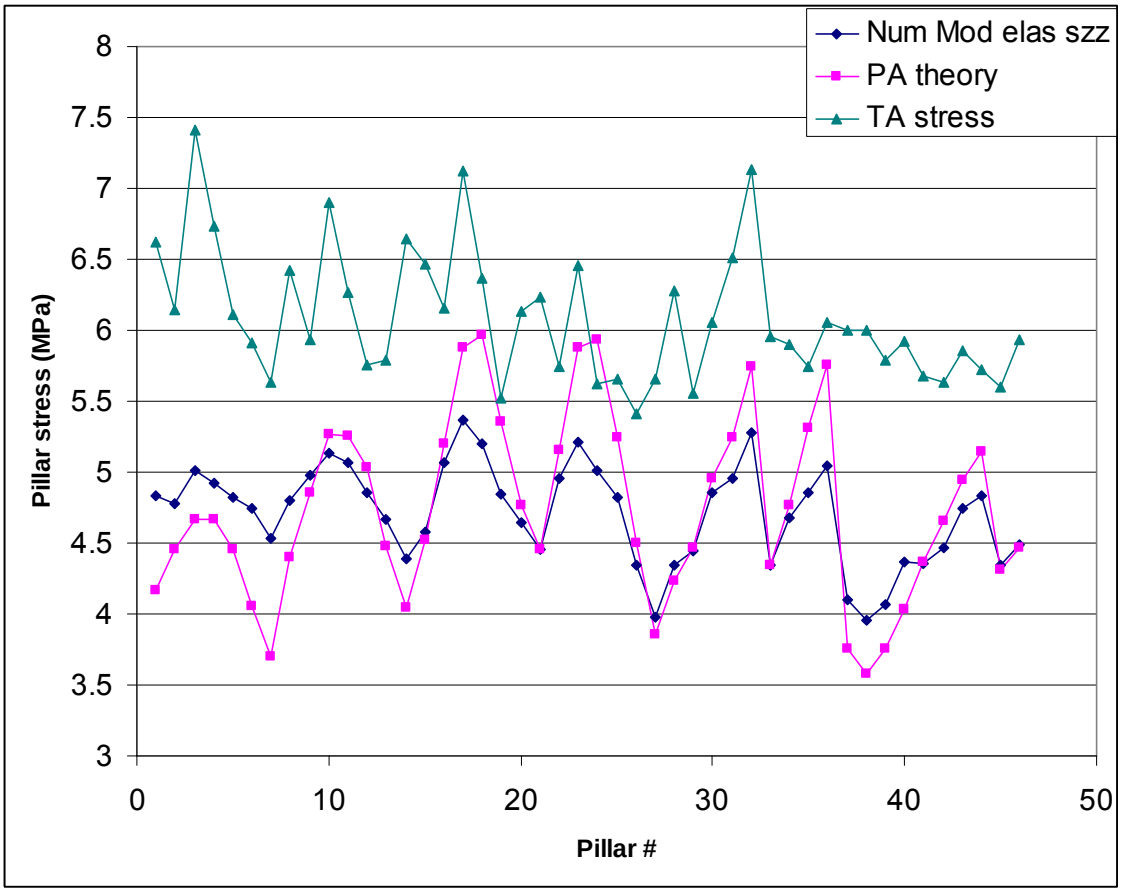

Figure A-5 Predicted pillar stress from numerical model of Duncan St region, Pressure Arch (PA) theory and Tributary Area (TA) theory. TA theory with constant bord width of 6.6m (mine plan shows 6.6m+ bord). Average absolute stress difference is 0.3MPa for PA theory and 1.4MPa for TA theory.

A.3 BENCHMARKING OF NUMERICAL MODEL

The pillar strength equation derived from the combined databases of Australia and South Africa is used to benchmark the numerical model. This equation, which is the same as equation (3) above, rewritten for convenience:

$$\text{Pillar strength} = 6.88\, w^{0.50} / h^{0.70} \qquad (3)$$

A typical pillar from the Duncan St region of Collingwood Park has a side length of 20m, internal acute angle in the range of 50-54 degrees. The excavation or pillar height is 6m+ and depth of cover is 124m, as shown in the mine pillar plan of Figure A-6.

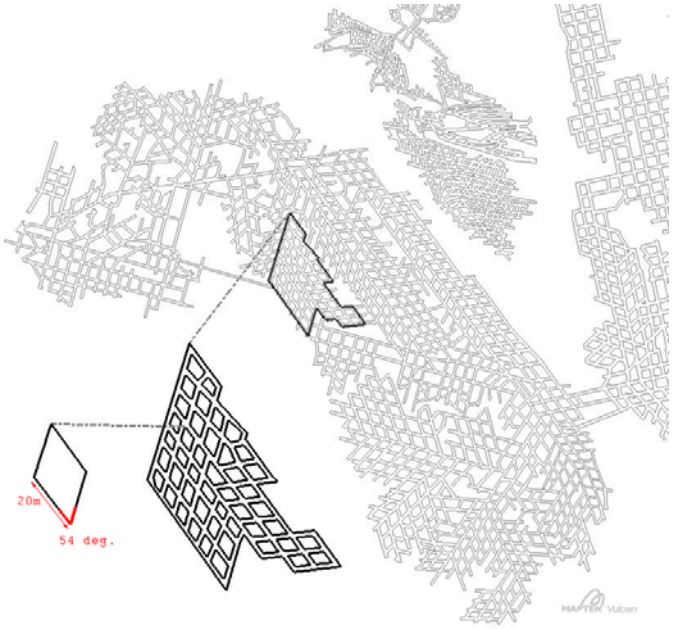

Figure A-6 Typical pillar with dimensions in the Duncan Street subsidence region. Highlighted outline is the location of the 3D model. Depth of cover is approximately 124m and pillar height is 6m+.

The code FLAC3D (F3D) by Itasca Consulting Group [Itasca, 2006] has been used for all numerical models. F3D is a continuum code with yield criteria suitably flexible for modelling the full stress/strain response of coal type materials. Only a quarter section of the bord and pillar array needs to be modelled, once symmetry conditions are enforced in both *x* and *y* directions, as shown in Figure A-7. Notice that only partial parts of the roof and floor have been considered.

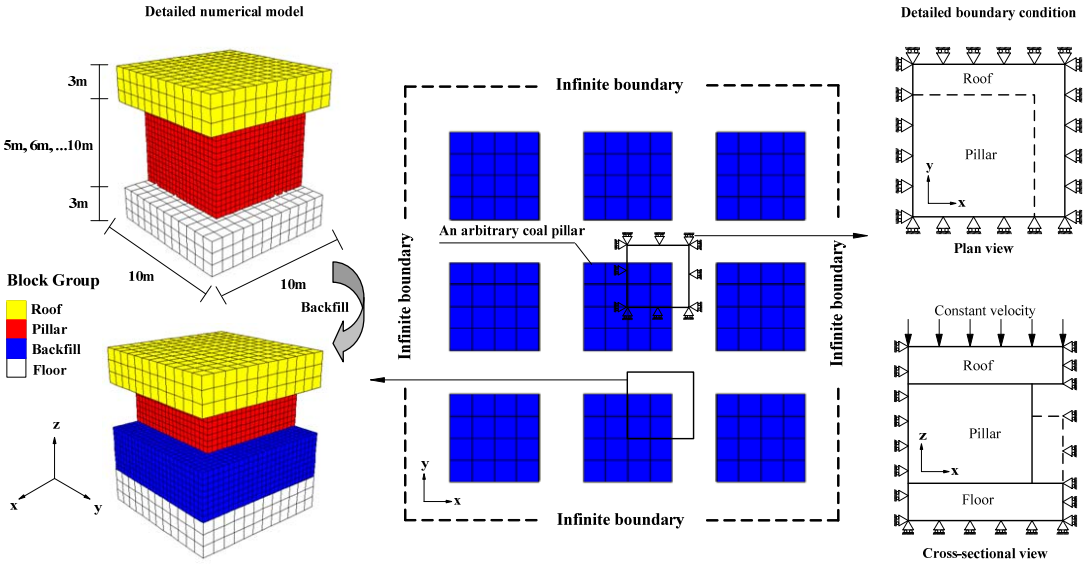

Figure A-7. A sketch of F3D mesh showing a quarter of a pillar as well as roof and floor and boundary conditions.

A strain softening yield criterion has been used for coal and rock materials modelling. In other words, Mohr-Coulomb material model with non-associated shear and associated tension flow rules [Fama, 1995; Itasca Consulting Group Inc., 2006; Pietruszczak, 1980; Hoke, 1990] has been used. In this model the parameters representing material cohesion, friction, dilation and tensile strength may reduce or soften after the onset of plastic yield by a user defined piecewise linear function [Jiang, 2009; Zhou, 2009], as displayed in Figure A-8. It is assumed that the roof and floor rock masses are elastic and only coal pillar is allowed to behave both elastically and plastically. All model material parameters are listed in Table A-1. To achieve a reasonable match with the strength formula of Equation (3) for a width to height ratio greater than 4, it was found that it is necessary to have an explicit yielding interface or joint at the pillar boundaries on both the roof and the floor contact areas. The interface properties are listed in Table A-2.

Coal properties for the numerical model are estimated from the reported literature values and from calibration analyses by matching Equation (3) for the range of width-to-height ratios from 2 to 4. These numerical results are compared with Equation (3) in Figure A-9.

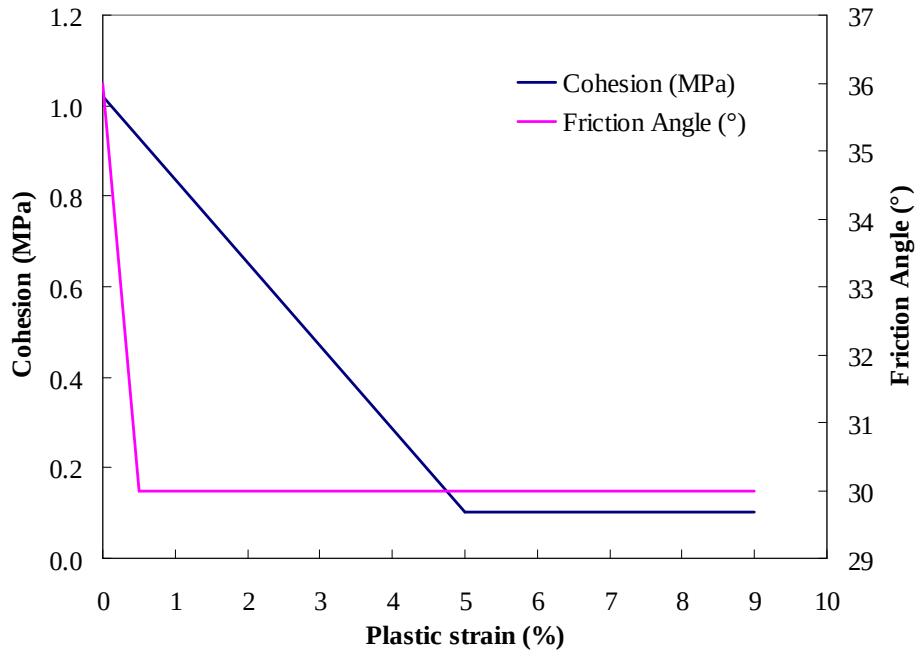

Figure A-8 Variation of cohesion and friction angle with plastic strain.

Table A-1. Mechanical parameters used in numerical models

Property	Young's Modulus (GPa)	Poisson's ratio	UCS (MPa)	Tensile Strength (MPa)	Cohesion			Friction Angle			Dilation Angle (°)
					Original value (MPa)	Softening rate (%)	Residual value (MPa)	Original value (°)	Softening rate (%)	Residual value (°)	
Coal	1.10*	0.30	4.0	0.04	1.02	5	0.102	36.0*	0.5	30.0	6.0
Roof	5.70	0.19	\	\	\	\	\	\	\	\	\
Floor	7.97	0.24	\	\	\	\	\	\	\	\	\

* from CSIRO report #42; Roof and floor materials are assumed elastic.

Table A-2. Mechanical parameters of interface used in numerical model

Interface property	Normal stiffness (GPa)	Shear stiffness (GPa)	Cohesion (MPa)	Friction Angle (°)
Value	2.0	2.0	0.5	20.0

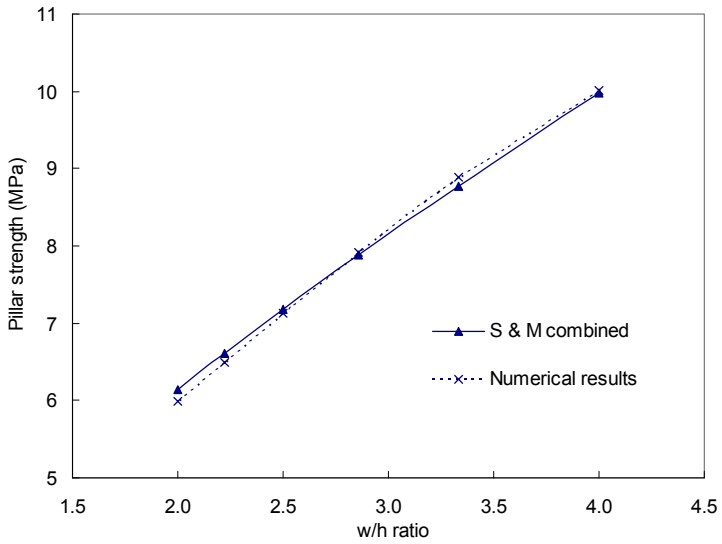

Figure A-9 FLAC^{3D} parametric study to match pillar strength with the analytical formula of Salamon & Munro (combined Australian and South African version).

A.4 PILLAR STRENGTH INCLUDING FULL STRESS STRAIN CURVE AND PILLAR SHAPE EFFECTS

A.4.1 Post peak strength

Das [Das, 1986] has presented work on the post peak strength for Indian coals at various width-to height ratios. His results show some variability but have a general correlation between post peak strength and increasing w/h ratio. Beyond a certain w/h ratio of approximately 5 to 8 Das's results predict that samples start to harden with increasing strain.

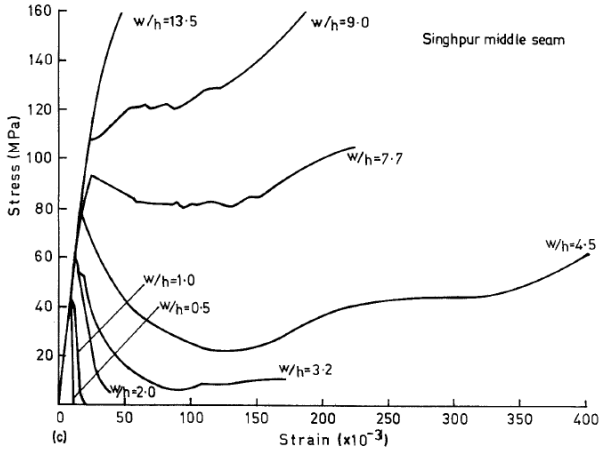

Figure A-10 Post peak strength of Indian coal at various width-to-height ratio, after Das 1986.

The numerical model of a square pillar of side length 20m and variable height was compressed to approximately 10% strain to investigate post peak behaviour with increasing w/h ratio for comparison with results of Das in Figure A-10. The numerical results are plotted in Figure A-11 for various width to height ratios in the range of 10% strain. The post peak pattern is similar to those of Das in Figure A-10, although the numerical hardening starts at lower strains.

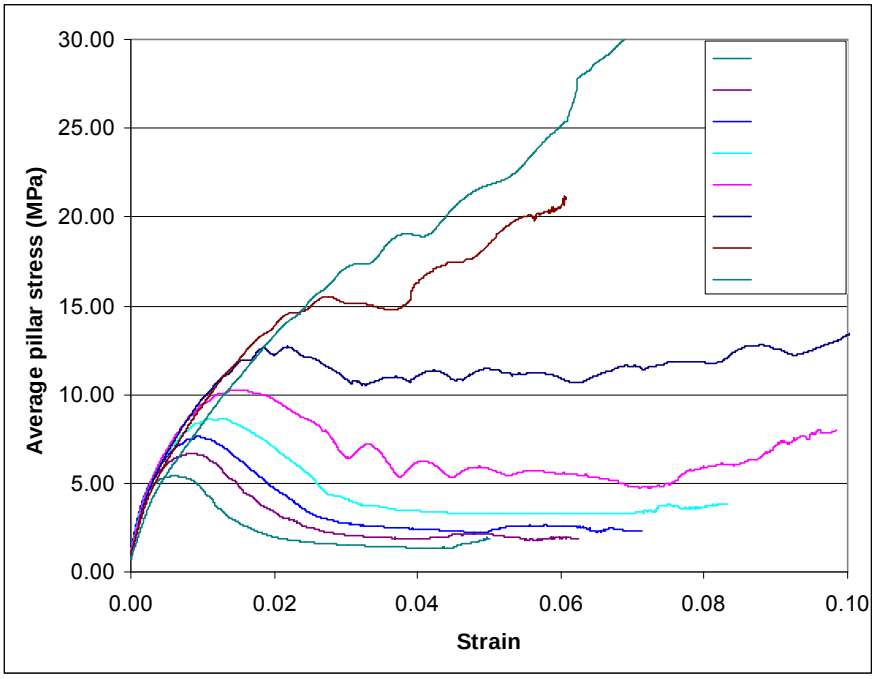

Figure A-11 Post peak failure behaviour of numerical pillars of constant width, w = 20m, but variable height (h).

Results from the modelling of the full stress strain curve of a 20m square pillar is used to estimate the stress redistributed to neighbouring pillars in the empirical estimation of pillar FoS for the CSIRO Hazard Maps. At 4% strain the percentage of peak strength carried by the coal pillar is approximated from Figure A-11 in Figure A-12 where conservatively it is assumed pillars cannot harden but only soften or retain strength.

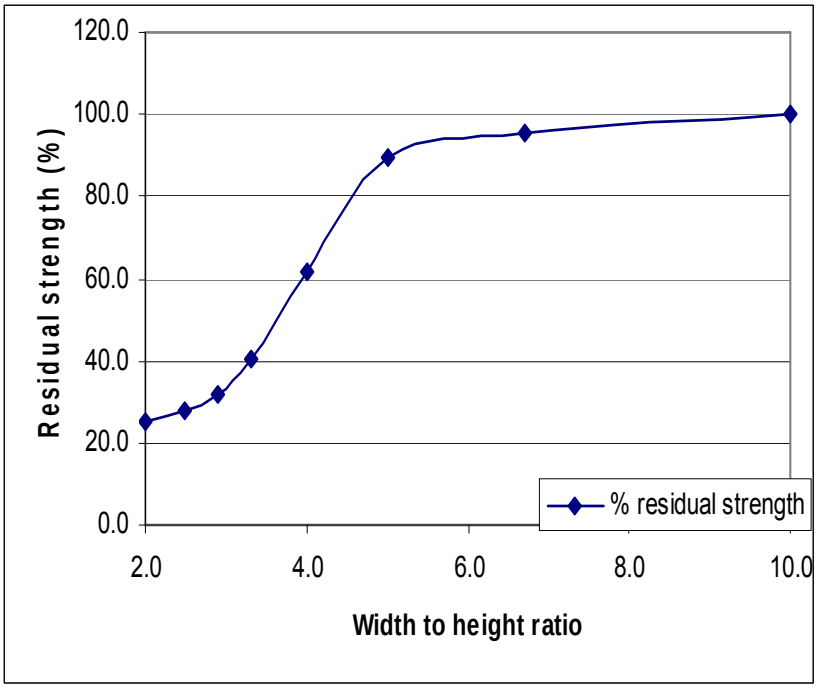

Figure A-12 Estimation of pillar residual strength at 4% strain.

A.4.2 Pillar shape influence on strength

Collingwood Park has many pillars of regular and irregular shapes, including square, rectangle, diamond, triangular and other polygon shapes. A study of some of these shapes at fixed 6m mining height was conducted.

As discussed in [Galvin 1981] with reference to physical models, there is a subtle difference in model response at specific width to height ratios, depending on whether the width or height of the model is fixed. This variation is attributed by Galvin to volume, stiffness and pillar end effect variation between width and height changes. In the Collingwood Park single pillar studies, generally the width is fixed at 20m and width-to-height changes are achieved with height variations and material properties are calibrated to this. In studies of diamond and other shaped pillars where the width or effective width varies a unique set of material properties calibrated over width-to-height 2 to 4 at fixed height is developed, Table A-3.

Attempt is made to keep the constant 0.5m cube element size although for some of the shapes studied this is not possible and where meshing options exist priority is given to minimizing the variability from the standard element size. Ideally the soften rate of the yield criteria would be adjusted based on an element characteristic length. Implementation of this reduced mesh dependent errors but it was not felt sufficiently rigorous for inclusion in this report.

Table A-3 Cohesion and friction for calibrated model at w/h 2 to 4 with fixed 6m pillar height.

Property	Cohesion			Friction Angle			Dilation Angle (°)
	Original value (MPa)	Softening rate (%)	Residual value (MPa)	Original value (°)	Softening rate (%)	Residual value (°)	
Coal	1.23	3.5	0.23	36.0	0.5	30.0	6.0

Diamond shaped pillars

Diamond pillar shapes located at Duncan St and adjacent areas have typical dimensions of side length 20-30m and minimum acute internal angles of 50 degrees.

The area perimeter or circumference (C) of a diamond shape is given by:

$$\text{Circumference} = C = 4\,w$$

where w is the side length. If the acute internal angle is θ, the area can be calculated as follows:

$$\text{Area} = A = w^2 \sin\theta$$

The minimum width or thickness of the cross section is:

$$\text{Minimum width} = w \sin\theta$$

Hence, the effective width, w_{eff}, from the analogy of "hydraulic radius = 4A/C", defined earlier is given by:

$$w_{eff} = 4A/C = w \sin \theta = \text{minimum width}$$

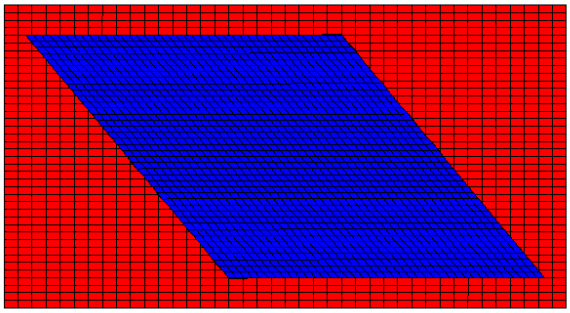

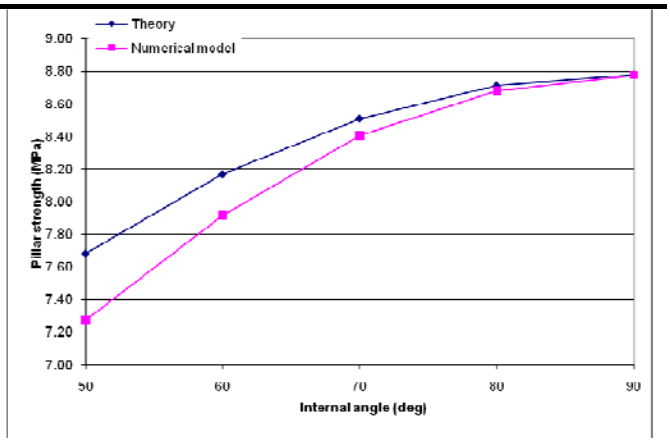

Figure A-13 Predicted pillar strength for diamond shaped pillars at 6m mining height. Error at 50 deg internal angle is approximately 6%.

Polygon with one acute corner

Figure A-14 (a) and (b) show a comparison between theory and numerical model for a polygon with one acute angle.

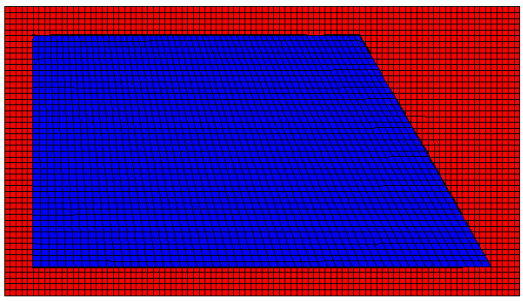

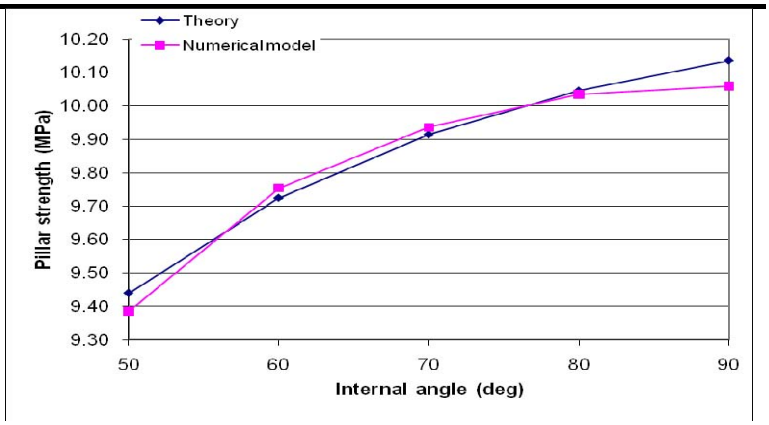

(a) (b)

Figure A-14 (a) Polygon with one acute side (60deg acute angle in figure). Base side length = 40m, short side, 20m, mining height = 6m and (w/h 4.4-3.8).

Rectangular pillar being split at mid-length in 1m increments

A rectangular pillar of 30m by 10m is modelled as it is split by a 5m roadway.

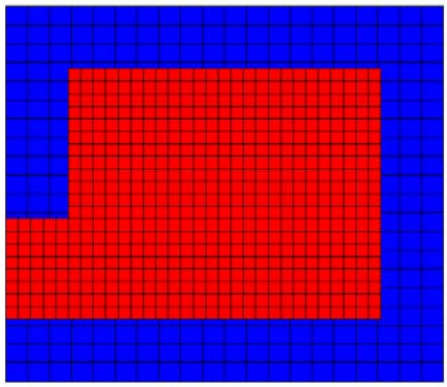

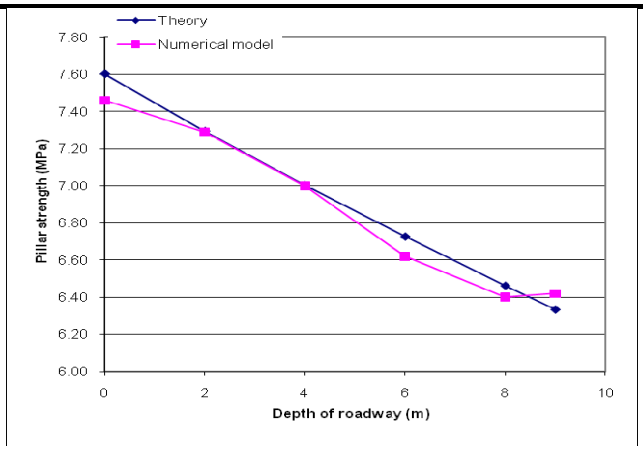

(a) (b)

Figure A-15 (a) Rectangle, 30m by 10m being split in 1m increments, Note symmetry plane on left hand boundary. Mining height 6m (b) Results from numerical model and Strength formula with w=4A/C.

Triangular shape pillars with two equal sides of 20m

In this example a triangular pillar with two sides of equal length of 20m is analysed.

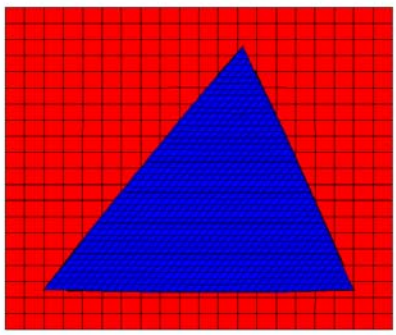

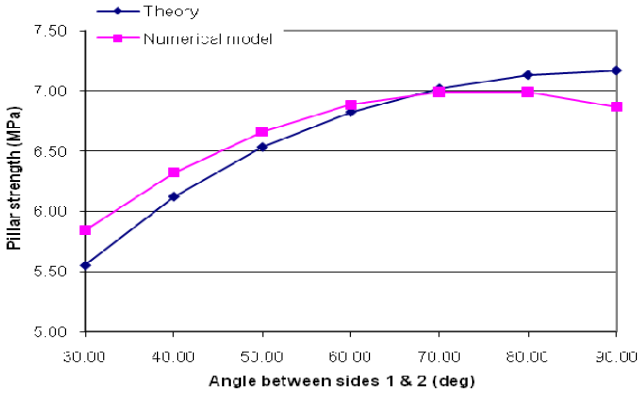

(a) (b)

Figure A-16 (a) Triangular pillar of two equal sides of 20m each. Mining height 6m (b) Results from numerical model and strength formula with w=4A/C. Maximum error is approximately 5%.

Observations from study of pillar shapes

The general conclusion from the study of pillar shapes at fixed 6m mining heights is that the hydraulic radius analogy of Wagner, Equation (4) where the effective width is estimated by area and circumference is applicable to pillars of Westfalen No. 3 colliery. Errors with this approach at calculating pillar width for width-to-height ratios from approximately 2 to approximately 4 for the shapes studied are under 6%.

A.4.3 Realistic roof geology

It is recognised that the idealised roof and floor of the pillar model, Figure A-7, may have an influence on the predicted strength estimation. To quantify this effect a model of a 20m square pillar at width-to-height ratio's of 2.2 to 4 is analysed with a realistic roof geology.

Based on the sonic logging data in borehole CP-C02 located in the failure region of Duncan Street, Figure A-17, pillar strength is estimated from a numerical model with the model input parameters selected from the scanned roof geological and geotechnical data. The input data are listed in **Error! Reference source not found.** and Table A-4. The F3D mesh for a pillar analysis is shown in Figure A-18 and the numerical results for two set of parameters for roof geology are shown in Figure A-19.

Table A-4. Mechanical properties of roof and overburden rocks

Backfill	Young's Modulus (GPa)	Poisson's Ratio	UCS (MPa)	Tensile Strength (MPa)	Cohesion (MPa)	Friction Angle (°)
Sandstone	13.5	0.12	25	2.5	6.648	40
Siltstone	19.5	0.20	15	1.5	4.728	38
Interbedded	16.6	0.17	20	2.0	2.808	38
Mudstone	8.75	0.26	10	1.0	1.943	30

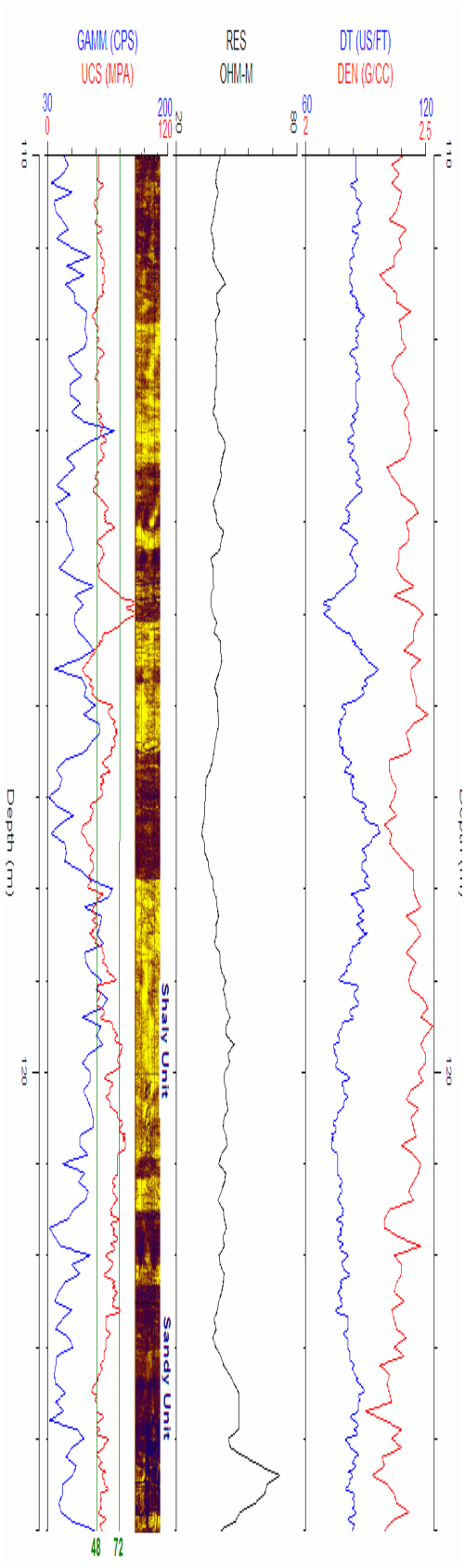

Depth (m)	UCS (MPa)	Geology	Scaled UCS (MPa)
100.5	75.00	sandstone1	25.00
101.0	60.00	interbedded1	20.00
101.5	67.50		22.50
102.0	75.00	sandstone2	25.00
102.5	90.00		30.00
103.0	67.50	interbedded2	22.50
103.5	45.00	siltstone1	15.00
104.0	52.50	interbedded3	17.50
104.5	45.00	siltstone2	15.00
105.0	22.5	coal1	7.50
105.5	22.50		7.50
106.0	82.50	sandstone3	27.50
106.5	90.00		30.00
107.0	37.50	siltstone3	12.50
107.5	52.50		17.50
108.0	60.00	interbedded4	20.00
108.5	60.00		20.00
109.0	37.50	siltstone4	12.50
109.5	30.00		10.00
110.0	30.00	mudstone1	10.00
110.5	30.00		10.00
111.0	37.50		12.50
111.5	45.00	siltstone5	15.00
112.0	37.50		12.50
112.5	20.00	coal2	6.67
113.0	52.50	interbedded5	17.50
113.5	75.00	sandstone4	25.00
114.0	60.00	interbedded6	20.00
114.5	52.50		17.50
115.0	82.50		27.50
115.5	90.00		30.00
116.0	105.00		35.00
116.5	135.00		45.00
117.0	105.00	sandstone5	35.00
117.5	101.25		33.75
118.0	105.00		35.00
118.5	97.50		32.50
119.0	75.00		25.00
119.5	37.50	siltstone6	12.50
120.0	15.00	coal3	5.00
120.5	78.75	sandstone6	26.25
121.0	86.25		28.75
121.5	52.50	interbedded7	17.50
122.0	90.00	sandstone7	30.00
122.5	105.00		35.00
123.0	60.00	interbedded8	20.00
123.5	30.00	mudstone2	10.00
124.0	37.50	siltstone7	12.50

Figure A-17 Sonic log of borehole CP-C02 and roof geological interpretation

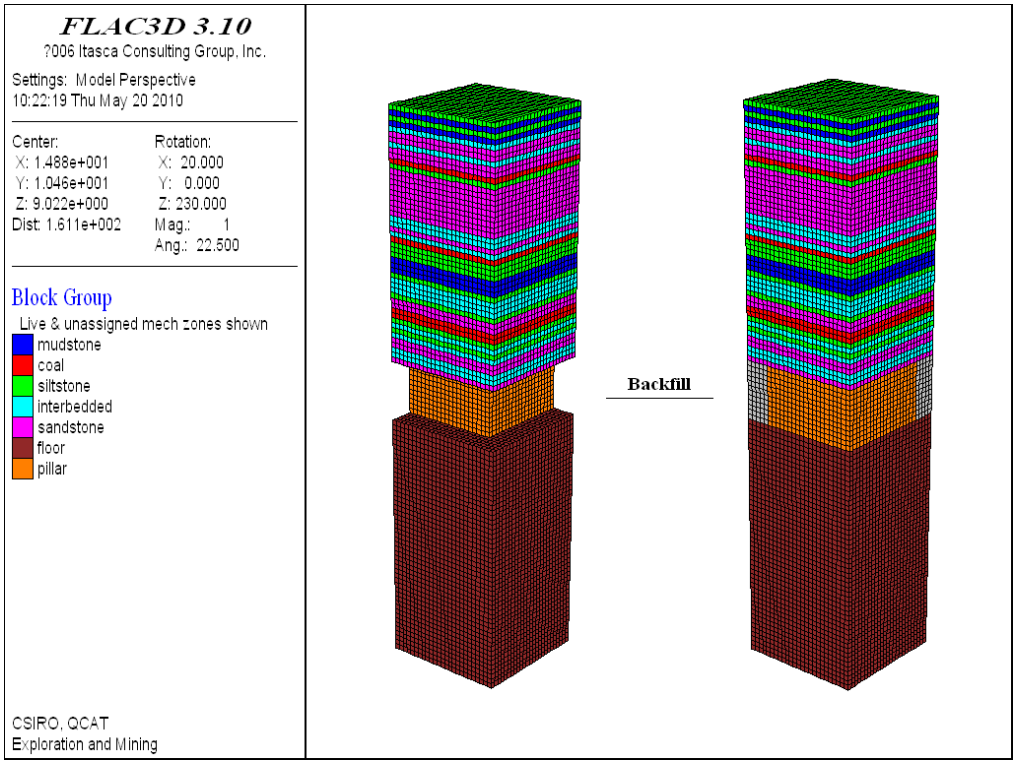

Figure A-18 Numerical model of a coal pillar with representative floor and roof rock geology

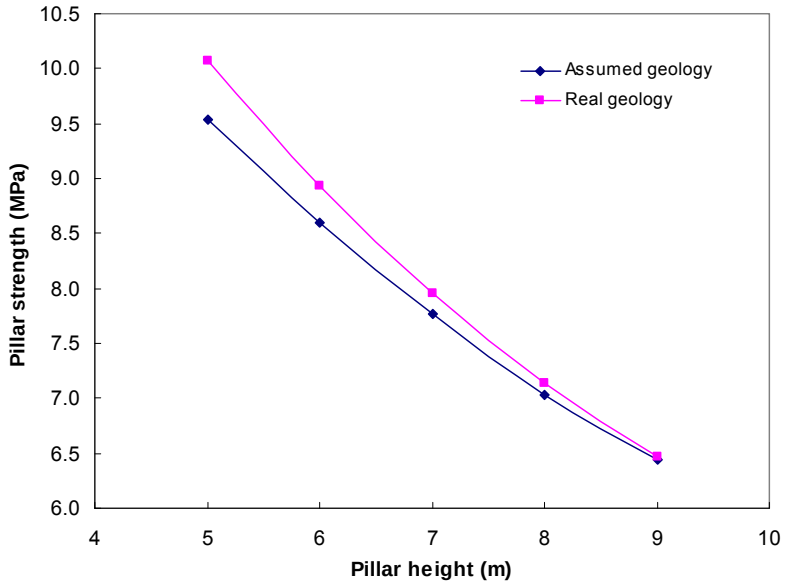

Figure A-19 Comparisons of pillar strength versus pillar height for realistic and simplified roof geology. Maximum error is 4.5%.

Modelling predicted that the maximum difference in pillar strength for two different roof geology conditions is approximately 4.5% at the lower height of 6m reducing to less than 1% for pillars of 9m mining height.

It is concluded from this study that the simplified roof and floor model satisfactorily estimates pillar strength allowing in excess of 180 numerical models to be analysed in a timely manner.

A.4.4 Pillars surrounded by roadways of variable height

It was observed in the 1983 pillar site investigation [Hollingworth, Dames & Moore, 1990] that mining heights at Westfalen No. 3 are extremely variable with roadways surrounding individual pillars varying by up to 2m.

To investigate the strength of pillars of variable height a 20m wide square model pillar of 8m mining height on one side and 6m height on the directly opposite side of the pillar, as shown in Figure A-20, has been analysed.

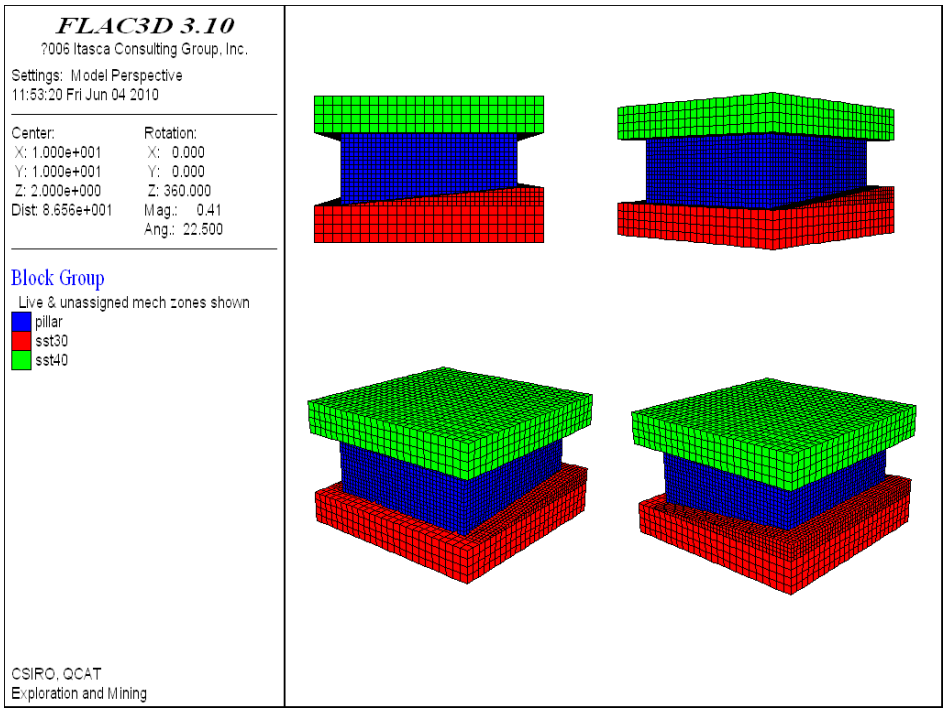

Figure A-20 Different views of the numerical modelling mesh of a trapezoidal-square pillar - Model is 8m high on one side and 6m on the other opposite side

Predicted strength of the variable height pillar together with stress-strain curves for pillars of 6m, 7m and 8m mining heights presented in Figure A-21. As shown in the figure, the predicted strength of a non-uniform-height pillar of trapezoidal shape having 6m and 8m side heights, approximates a uniform-height pillar with a constant height of 7m.

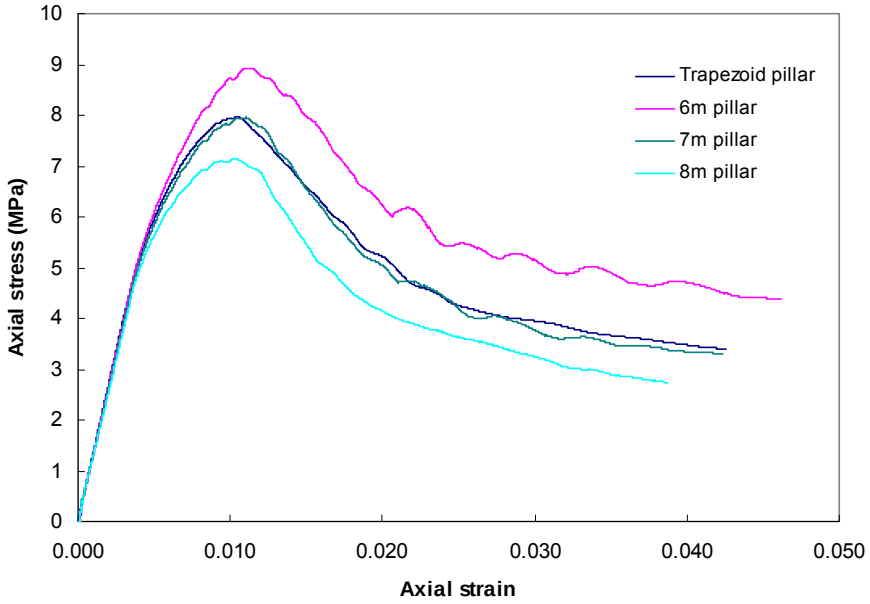

Figure A-21 Stress vs strain curves for rectangular uniform height and trapezoidal non-uniform height pillars. Strength of uniform pillars having heights of 6m, 7m and 8m are compared with a trapezoidal non-uniform height pillar of having 6m height on one side and 8m on the other opposite side, i.e. a variable height roadway of average 7m height.

A.4.5 Pillars created by multiple passes to variable depth

Roadways at Westfalen No. 3 colliery were cut in multiple passes at a constant height of 2.4 m. The cut widths were variable ranging from 5.2 m at the bottom to 7.6 m at the top, as shown schematically in Figure A-22, by the mine manager's hand drawings of the roadway mining method.

To asses the strength of such pillars, a 9 m high pillar with irregular side surface boundary is modelled, Figure A-23. The model pillar has a square base of 23m and side length with three 'cuts' in its height, as shown in Figure A-23.

Predicted strength is approximately equal to a similar pillar with effective width equal to minimum width, ie 20m in this case, Figure A-24.

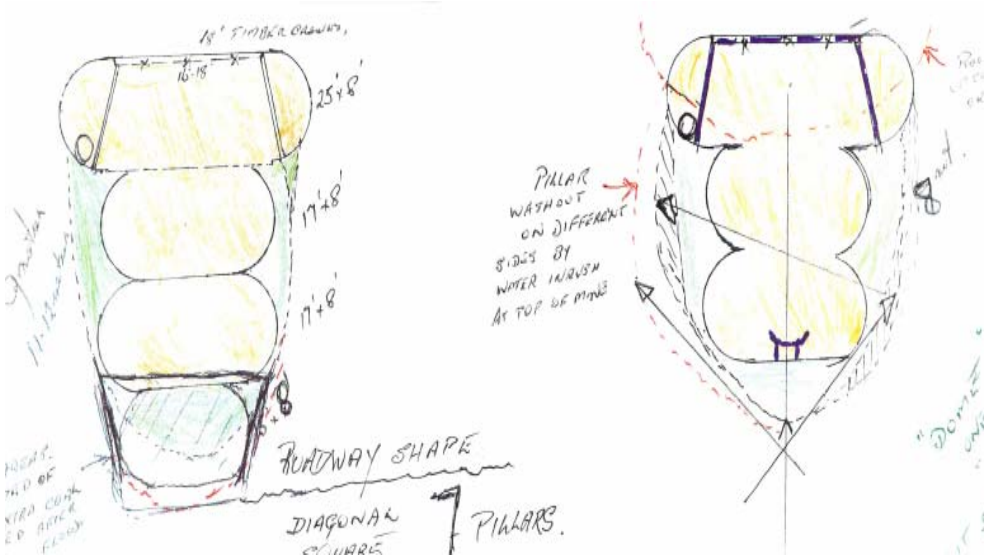

Figure A-22 Sketch of roadways at Collingwood Park showing multiple passes or layers of cutting of the coal seam.(from previous mine managers' notes and records)

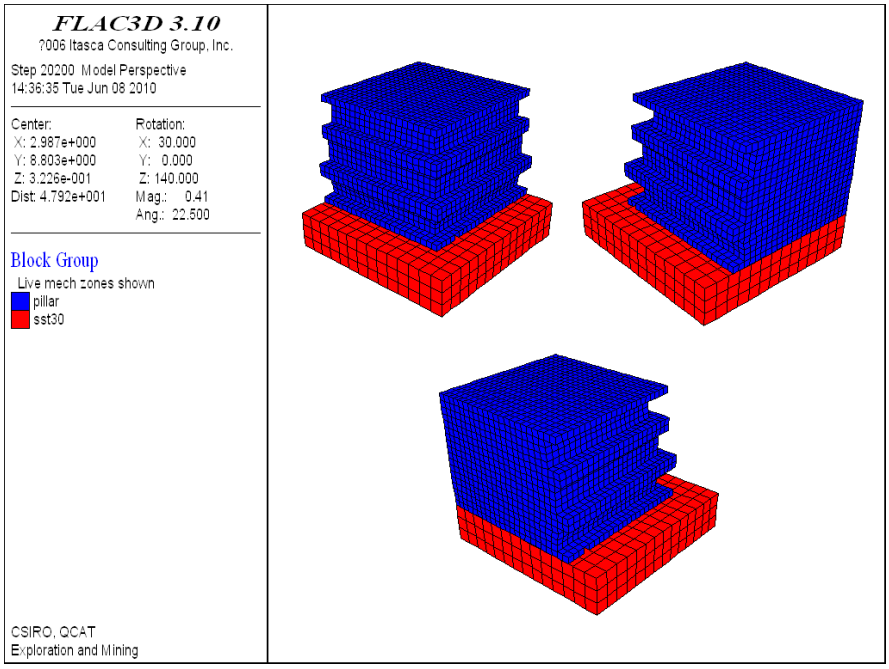

Figure A-23 Numerical modelling of a multi-pass cut pillar of 9 m height with minimum and maximum side widths of 20m and 23m, respectively.

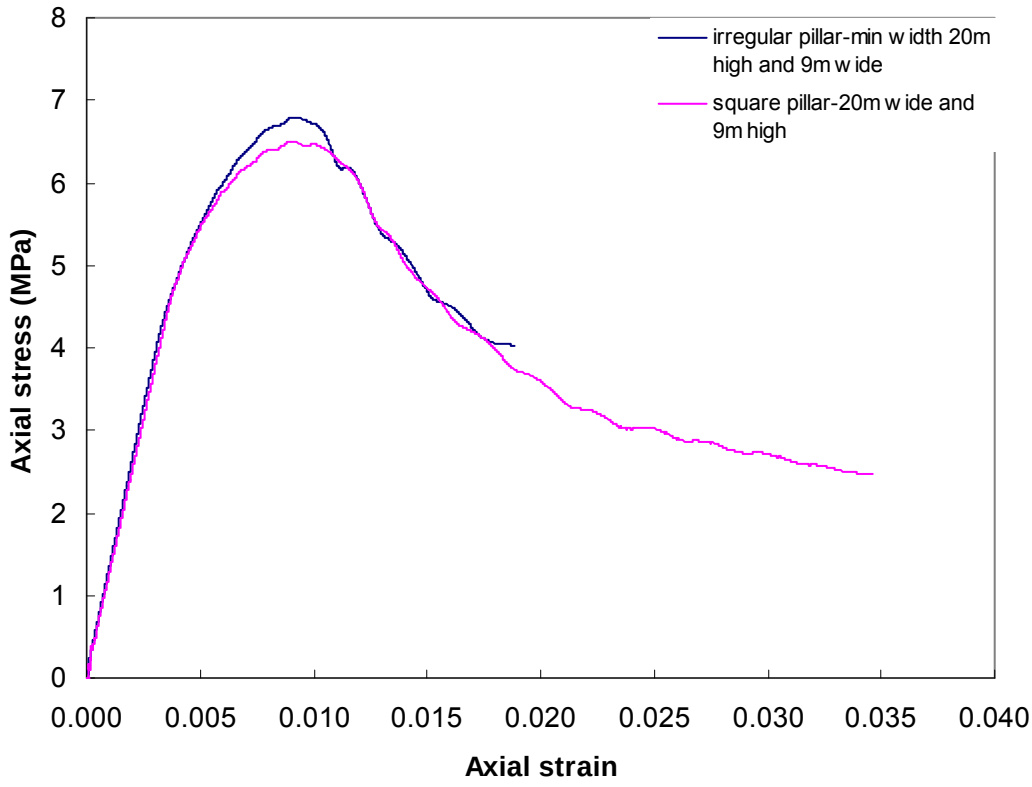

Figure A-24 Stress vs strain curves for pillars of 9m height with regular and irregular square cross-section (Figure A-23). Difference in peak strength predicted to be approximately 3.5%.

A.5 ROADWAY BACKFILL AND PILLAR STRENGTH IMPROVEMENT

A literature review of backfill applications, mechanical properties and behaviours in coal mining identified several examples from China [Guo, 2007; Wang, 2009] where backfill has been used to reduce surface subsidence, from America [Tesarik, 2002; 2009], where backfill has been used primarily for disposal of fly-ash and reduce acid mine drainage and from Australia [Origin Alliance, 2008], - See Table A-5 and the reference list.

In the early stages of this modelling specific data and backfill effects and properties required in this numerical study were unavailable and therefore, two cases were considered, a cohesive backfill having a UCS of 1 MPa and a non-cohesive backfill with no cohesion but a friction angle of 42 degrees. Subsequent to these two cases, a case of 0.5MPa cohesive backfill mix was also considered.

Backfill properties using in this study are list in

Table A-6.

Table A-5 Backfill properties, data from various sources.

Composition	**UCS (MPa)**	**E (GPa)**	**Reference**
Solid waste including fly-ash	0.5 initially to 1.4-1.7	0.565	Guo et al, 2007
Fly-ash & cement	3.39 – 8.24		Guo et al, 2007
1 : 4 : 15 (cement) : (fly-ash) : (coal gangue)	0.7 – 1.7		Wang et al, 2009
Fly ash (dry)			Scheetz, 2009
2.2 : 1 (fly-ash) : (cement)			Scheetz, 2009
Cemented rockfill in metal mine	6.9	1.909	Tesarik, 2009
Required properties	1.0	1.0	OriginAlliance – Mine subsidence interpretive reporting P16
2.5 FA : 10.5 sand : 0.1 bentonite 5 FA : 18 sand Injection 3m intervals			Bell Bruyn, 1999

Table A-6 Mechanical parameters of cohesive and non-cohesive backfill used in this numerical study

Backfill	Young's Modulus (GPa)	Poisson's Ratio	UCS (MPa)	Tensile Strength (MPa)	Cohesion (MPa)	Friction Angle (°)	Dilation Angle (°)
1MPa Cohesive	0.565	0.40	1.0	0.1	0.117	40.0	10.0
0.5MPa-cohesive	0.565	0.40	0.5	0.05	0.061	40.0	10.0
Non-cohesive	0.020	0.15	0.0	0.0	0.000	42.0	7.5

A.5.1 Numerical results and analysis

In order to quantify the influence of backfill on pillar strength in detail, 180 models (60 models each for 1MPa, 0.5MPa cohesive and non-cohesive backfill) of square coal pillars were analysed with the following parameters: pillar width is 20m, mining height is from 5m to 10m, equivalent to a w/h ratio of 2 to 4, percentage of backfill is from 0 to 90%. Table A-7 summarises the results of these pillar strength analyses for all the cohesive and non-cohesive cases.

Relationship between pillar strength and percentage of roadway backfill is presented in Figure A-25, Figure A-27 and Figure A-29. The raw data from Table A-7 has been calculated in uniform 10%

backfill increments and is presented in Figure A-26, Figure A-28 and Figure A-30. As shown in these figures, the percentage increase in pillar strength is approximately bilinear with increase in backfill.

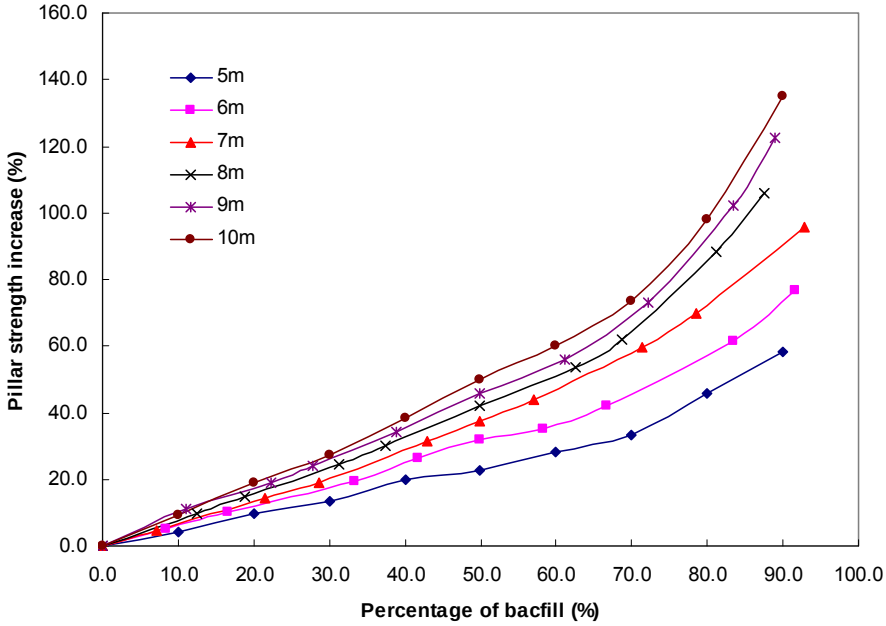

Figure A-25 Pillar strength increase versus percentage of 1MPa cohesive backfill.

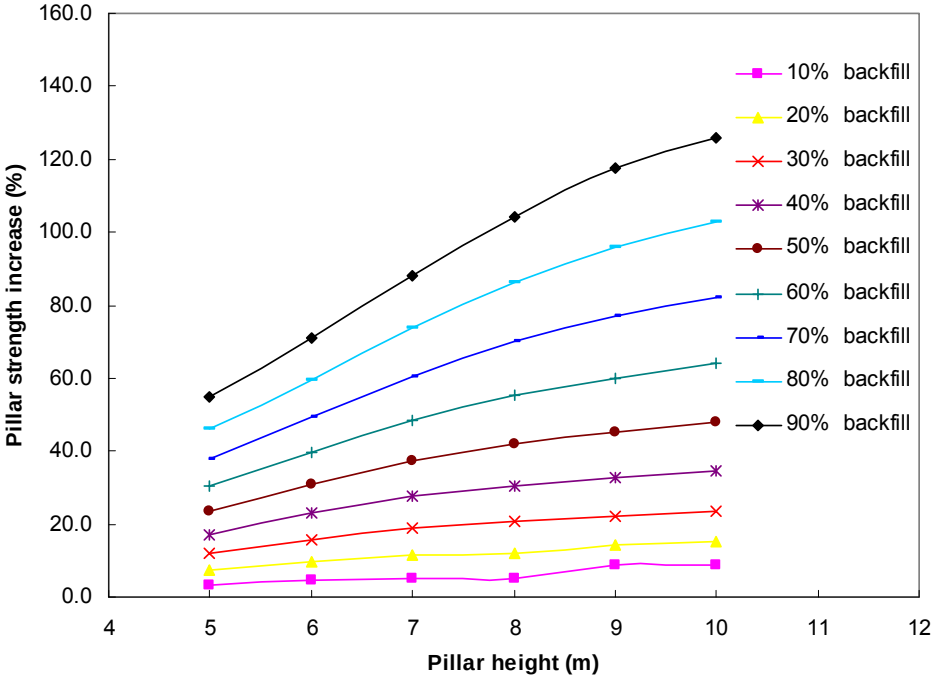

Figure A-26 Pillar strength increase versus pillar height for 1MPa cohesive backfill.

Table A-7 Pillar strength with increasing 1MPa and 0.5MPa cohesive backfill and non-cohesive backfill

Pillar strength	Backfill	Approximate percentage of backfill (%)	Pillar height (m)					
			5	6	7	8	9	10
Pillar strength (MPa) for different percent-age of backfill	Without backfill	0	10.07(0.0%)	8.94(0.0%)	7.95(0.0%)	7.14(0.0%)	6.47(0.0%)	5.96(0.0%)
	1MPa Cohesive backfill	10	10.49(10.0%)	9.40(8.3%)	8.33(7.1%)	7.85(12.5%)	7.20(11.1%)	6.50(10.0%)
		20	11.04(20.0%)	9.83(16.7%)	9.09(21.4%)	8.20(18.8%)	7.71(22.2%)	7.10(20.0%)
		30	11.40(30.0%)	10.69(33.3%)	9.47(28.6%)	8.89(31.3%)	8.03(27.8%)	7.58(30.0%)
		40	12.05(40.0%)	11.30(41.7%)	10.46(42.9%)	9.29(37.5%)	8.69(38.9%)	8.24(40.0%)
		50	12.34(50.0%)	11.78(50.0%)	10.95(50.0%)	10.16(50.0%)	9.43(50.0%)	8.94(50.0%)
		60	12.92(60.0%)	12.08(58.3%)	11.43(57.1%)	10.98(62.5%)	10.09(61.1%)	9.56(60.0%)
		70	13.42(70.0%)	12.71(66.7%)	12.70(71.4%)	11.58(68.8%)	11.20(72.2%)	10.35(70.0%)
		80	14.66(80.0%)	14.42(83.3%)	13.50(78.6%)	13.45(81.3%)	13.09(83.3%)	11.80(80.0%)
		90	15.93(90.0%)	15.80(91.7%)	15.56(92.9%)	14.70(87.5%)	14.40(88.9%)	14.00(90.0%)
	0.5MPa Cohesive backfill	10	10.26(10.0%)	9.30(8.3%)	8.30(7.1%)	7.73(12.5%)	6.97(11.1%)	6.36(10.0%)
		20	10.81(20.0%)	9.68(16.7%)	8.96(21.4%)	8.03(18.8%)	7.54(22.2%)	6.87(20.0%)
		30	11.32(30.0%)	10.53(33.3%)	9.39(28.6%)	8.71(31.3%)	7.86(27.8%)	7.41(30.0%)
		40	11.84(40.0%)	10.98(41.7%)	10.18(42.9%)	9.01(37.5%)	8.53(38.9%)	7.99(40.0%)
		50	12.17(50.0%)	11.41(50.0%)	10.65(50.0%)	10.00(50.0%)	9.36(50.0%)	8.73(50.0%)
		60	12.40(60.0%)	11.67(58.3%)	11.02(57.1%)	10.54(62.5%)	10.09(61.1%)	9.54(60.0%)
		70	12.69(70.0%)	11.89(66.7%)	12.37(71.4%)	10.93(68.8%)	10.44(72.2%)	10.14(70.0%)
		80	13.22(80.0%)	12.80(83.3%)	11.67(78.6%)	11.43(81.3%)	11.05(83.3%)	10.61(80.0%)
		90	14.10(90.0%)	13.50(91.7%)	12.50(92.9%)	12.02(87.5%)	11.50(88.9%)	11.20(90.0%)
	Non-cohesive backfill	10	10.16(10.0%)	9.02(8.3%)	8.01(7.1%)	7.24(12.5%)	6.57(11.1%)	6.04(10.0%)
		20	10.28(20.0%)	9.12(16.7%)	8.19(21.4%)	7.32(18.8%)	6.70(22.2%)	6.15(20.0%)
		30	10.44(30.0%)	9.41(33.3%)	8.32(28.6%)	7.53(31.3%)	6.78(27.8%)	6.29(30.0%)

Pillar strength	Backfill	Approximate percentage of backfill (%)	Pillar height (m)					
			5	6	7	8	9	10
		40	10.63(40.0%)	9.61(41.7%)	8.65(42.9%)	7.67(37.5%)	7.02(38.9%)	6.49(40.0%)
		50	10.86(50.0%)	9.84(50.0%)	8.85(50.0%)	8.00(50.0%)	7.29(50.0%)	6.70(50.0%)
		60	11.13(60.0%)	10.06(58.3%)	9.04(57.1%)	8.35(62.5%)	7.60(61.1%)	6.96(60.0%)
		70	11.38(70.0%)	10.30(66.7%)	9.43(71.4%)	8.52(68.8%)	7.92(72.2%)	7.25(70.0%)
		80	11.68(80.0%)	10.83(83.3%)	9.63(78.6%)	8.89(81.3%)	8.29(83.3%)	7.65(80.0%)
		90	12.06(90.0%)	11.30(91.7%)	10.29(92.9%)	9.13(87.5%)	8.52(88.9%)	8.04(90.0%)

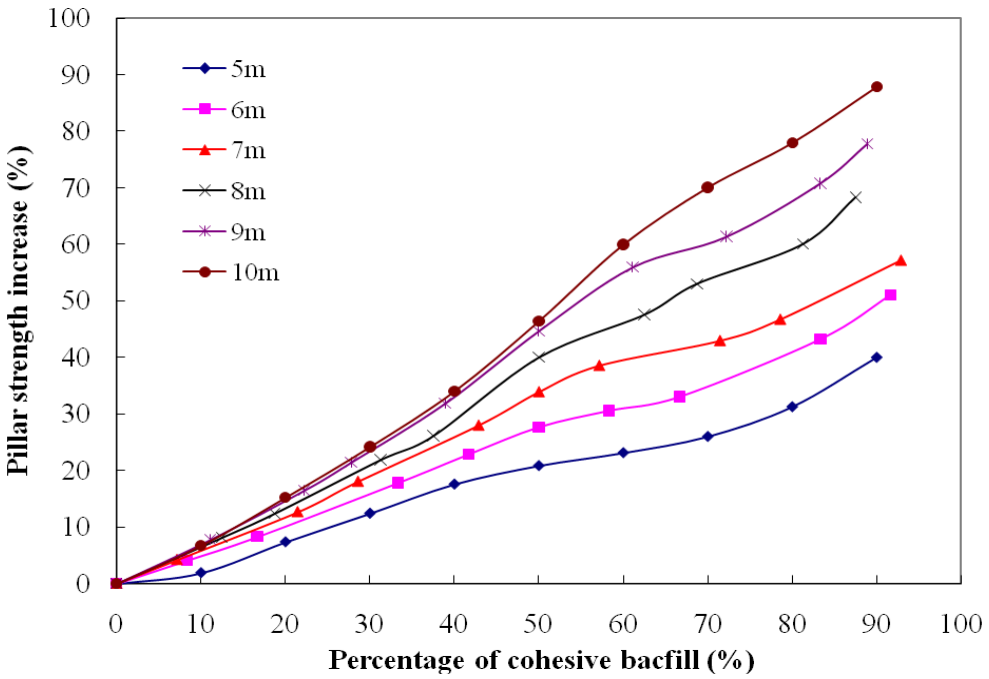

Figure A-27 Pillar strength increase versus pillar height for 0.5MPa cohesive backfill.

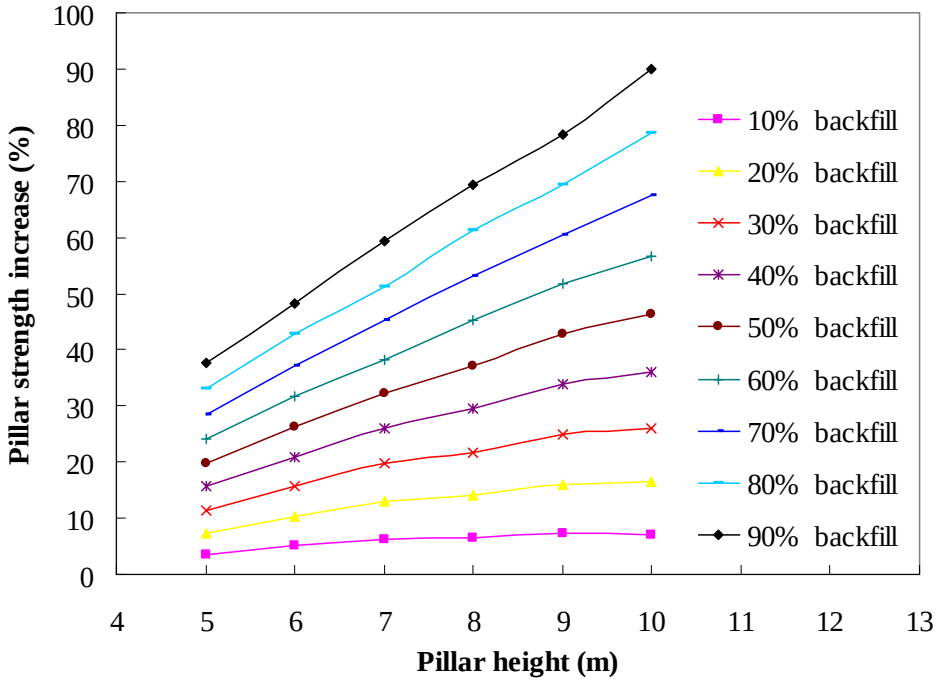

Figure A-28 Pillar strength increase versus percentage of 0.5MPa cohesive backfill

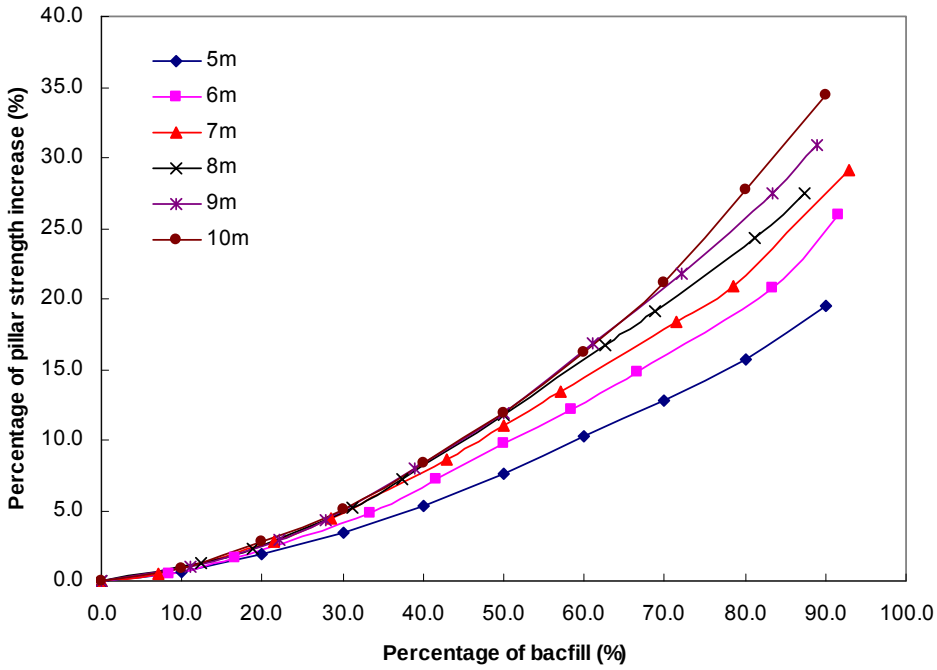

Figure A-29 Pillar strength increase versus percentage of non-cohesive backfill

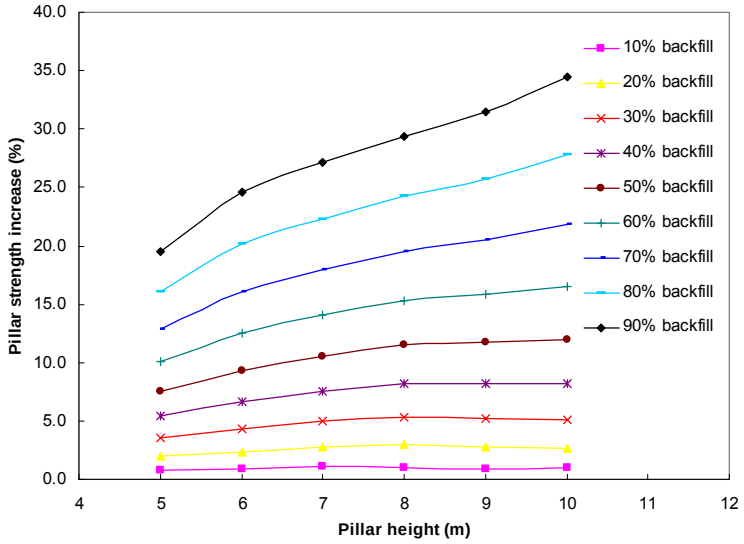

Figure A-30 Pillar strength increase versus pillar height for non-cohesive backfill

The modelling results suggest that the pillar strength will increase with increasing roadway backfill, while the percentage increase of pillar strength is greater for the taller pillars than squat pillars. it is observed that when the backfill is less than 40-50% the pillar strength increase is less sensitive to pillar height or w/h ratio, while over 40-50% backfill, pillar strength rapidly increase with pillar height.

A.5.2 Comparison of three different kinds of backfill

Pillar strength improvement with 0.5 and 1.0 MPa cohesive backfill and non-cohesive backfill is presented in Figure A-31 to Figure A-33.

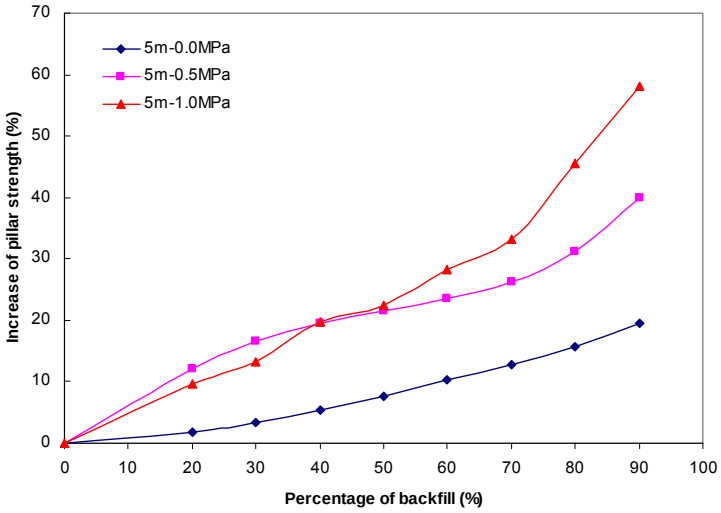

Figure A-31 Comparison of 0.5 and 1.0 MPa cohesive backfill and non-cohesive backfill at 5m mining height.

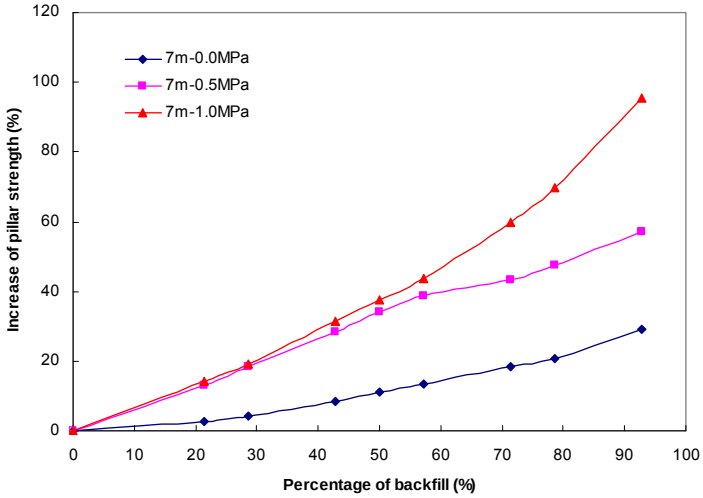

Figure A-32 Comparison of 0.5 and 1.0 MPa cohesive backfill and non-cohesive backfill at 7m mining height.

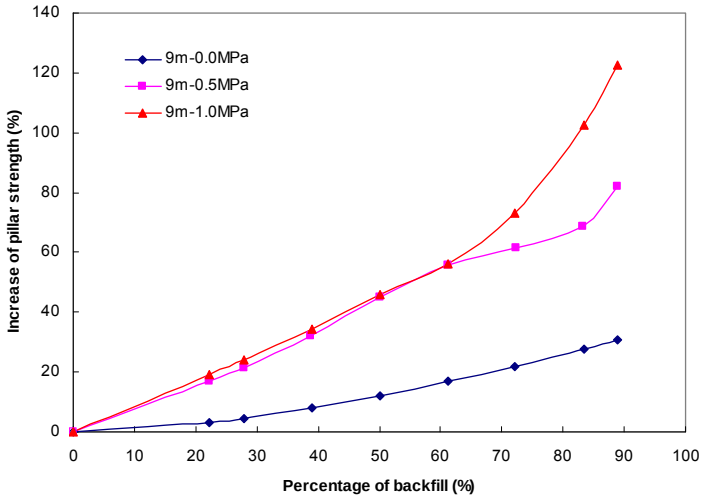

Figure A-33 Comparison of 0.5 and 1.0 MPa cohesive backfill and non-cohesive backfill at 9m mining height.

Modelling predicts that 0.5MPa is as effective as 1.0MPa at increasing pillar strength below approximately 50-60% roadway fill. Modelling suggests that cohesive backfill is more effective at increasing pillar strength than non-cohesive fill.

A.5.3 Numerical study of the influence of interface between backfill and pillar

To investigate the influence of an interface between backfill and pillar on the strength response of coal pillar, an interface is set between backfill and pillar, as shown in Figure A-34. The interface property is list in Table A-8.

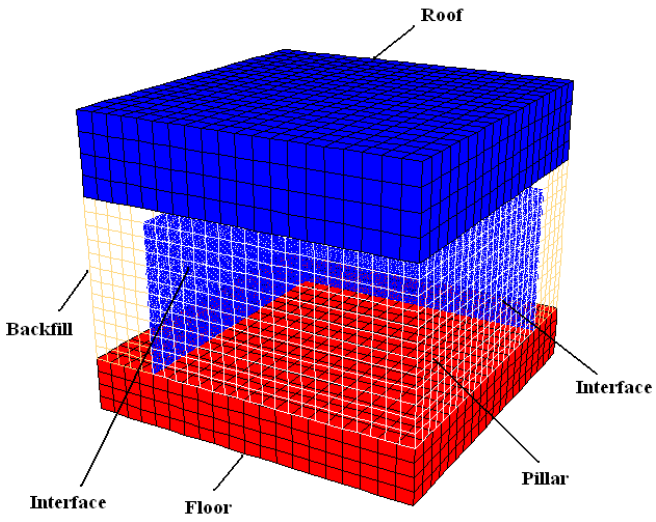

Figure A-34 Sketch showing the position of interface between backfill and pillar.

Table A-8 Mechanical parameters of interface used in numerical model

Interface property	Normal stiffness (GPa)	Shear stiffness (GPa)	Cohesion (MPa)	Friction Angle (°)
Value	2.0	2.0	0	5~40

Pillar strength of a 6m high pillar as interface friction angle is increased from 5 degrees to 40 degrees is displayed in

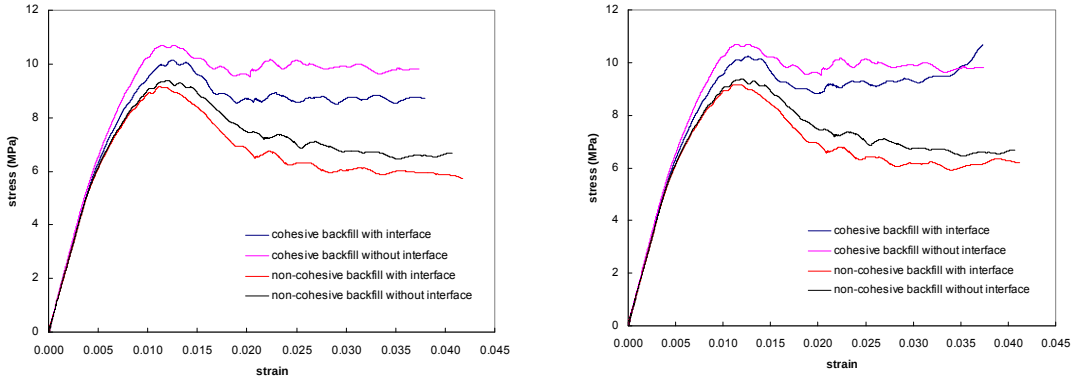

Figure A-35 to Figure A-38.

Modelling predicts a non-cohesive interface with friction angle below 20 degrees results in a slight reduction in pillar strength, above 20 degrees the interface is predicted to have little influence on pillar strength.

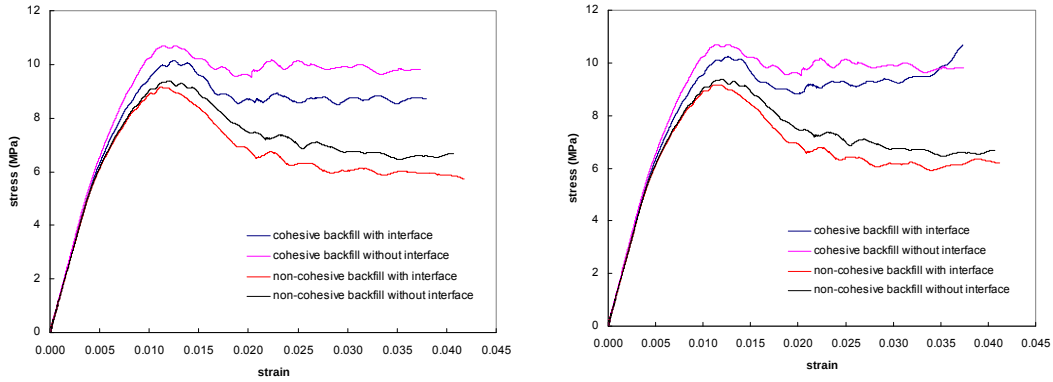

Figure A-35 Post peak pillar for 6m high pillar (w/h=3.3) with friction angle 5° on left 10° on right of interface between backfill and pillar.

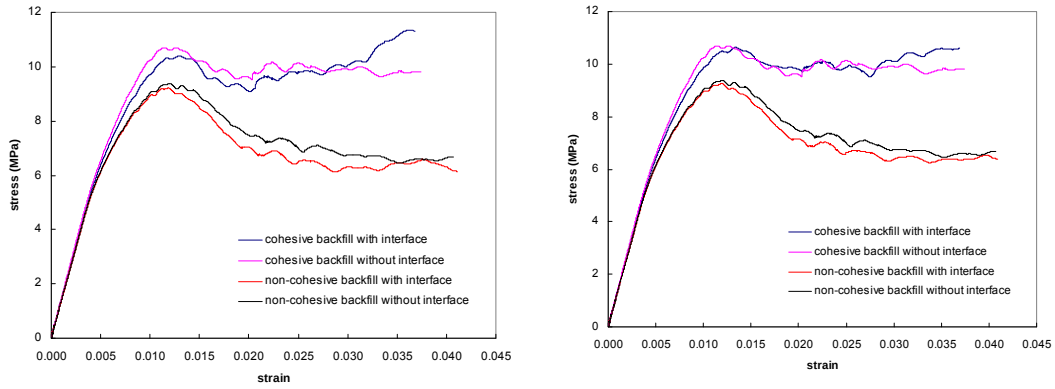

Figure A-36 Post peak pillar for 6m high pillar (w/h=3.3) with friction angle 15° on left 20° on right of interface between backfill and pillar.

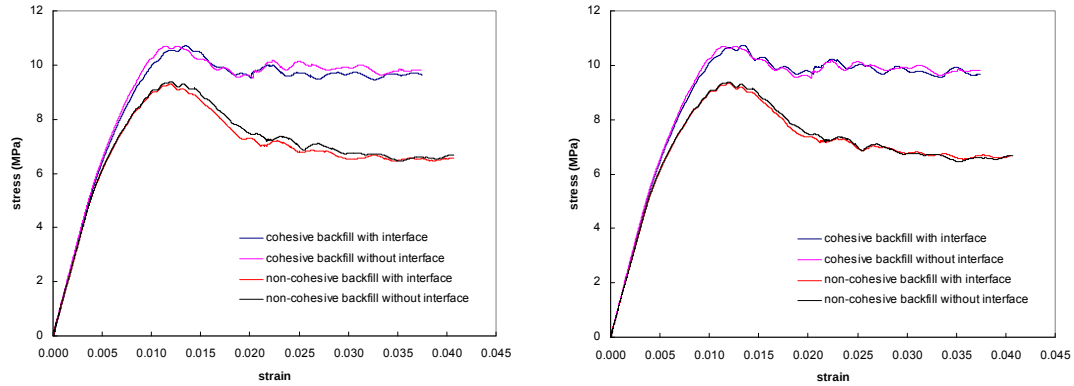

Figure A-37 Post peak pillar for 6m high pillar (w/h=3.3) with friction angle 25° on left 30° on right of interface between backfill and pillar.

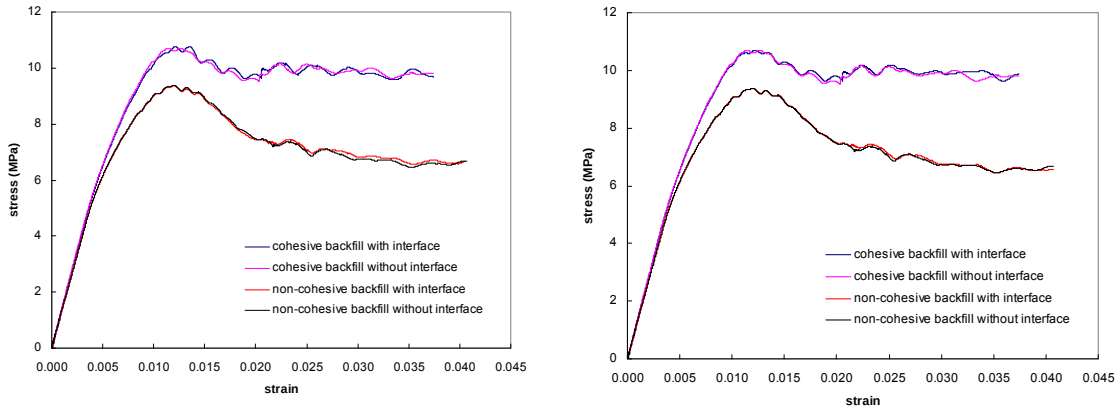

Figure A-38 Post peak pillar for 6m high pillar (w/h=3.3) with friction angle 35° on left 40° on right of interface between backfill and pillar.

A.5.4 Post peak pillar strength

A full stress strain curve to approximately 3.5% strain is presented in the following figures for 1MPa cohesive and non-cohesive backfill. Results for 0.5MPa cohesive backfill sit approximately mid-way between these two cases and are included in the summary Table A-9.

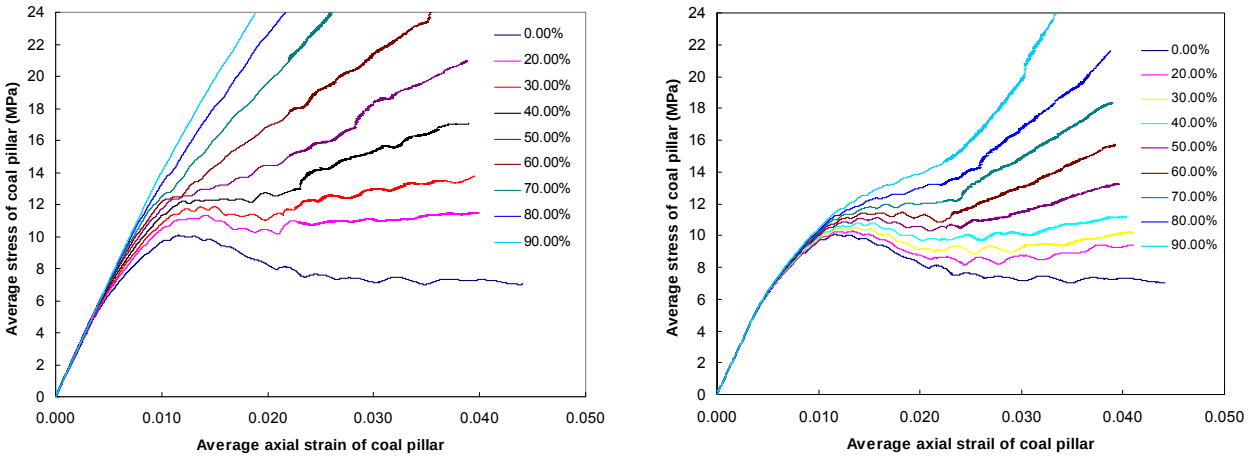

Figure A-39 Post peak pillar strength with increasing backfill. 5m high pillar (w/h=4.0) with 1MPa cohesive backfill on left non-cohesive backfill on right.

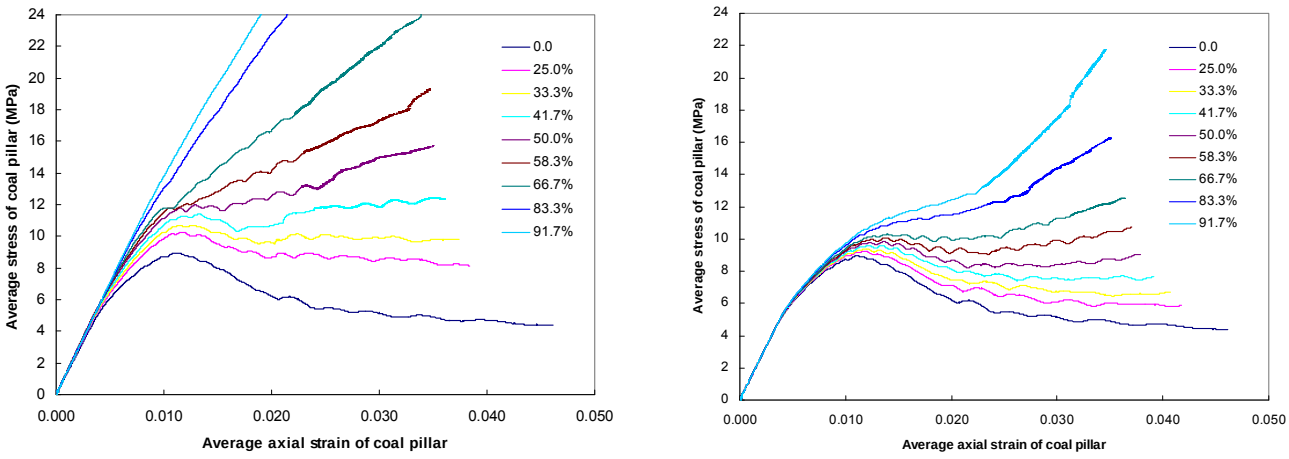

Figure A-40 Post peak pillar strength with increasing backfill. 6m high pillar (w/h=3.3) with cohesive backfill on left non-cohesive backfill on right.

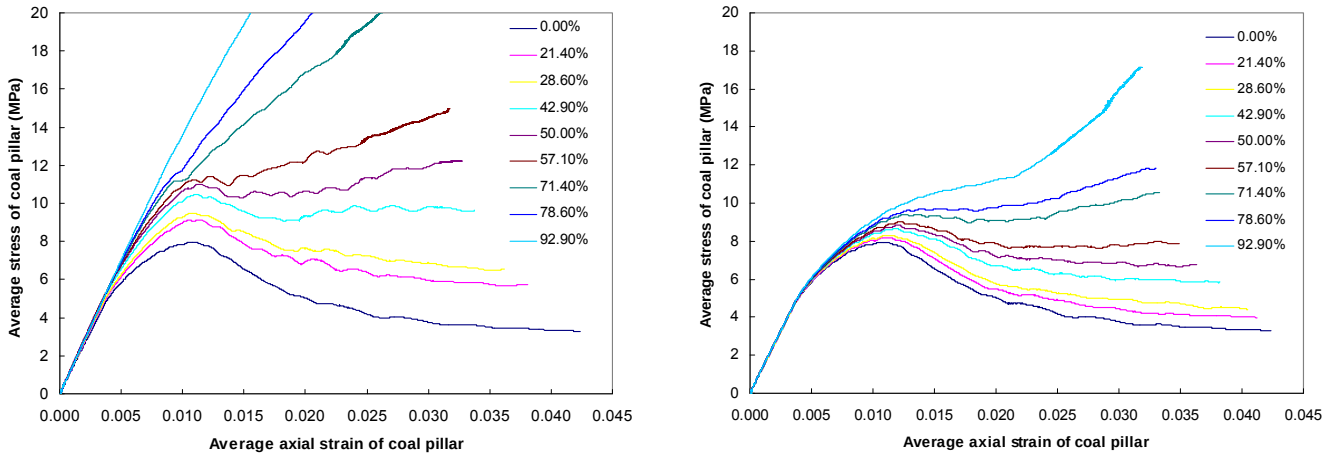

Figure A-41 Post peak pillar strength with increasing backfill. 7m high pillar (w/h=2.9) with cohesive backfill on left non-cohesive backfill on right.

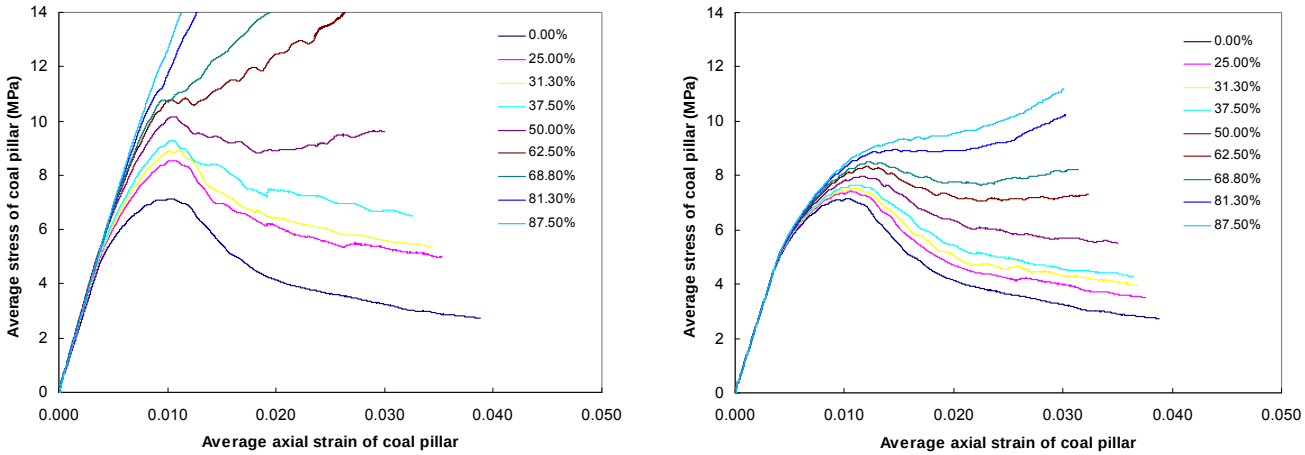

Figure A-42 Post peak pillar strength with increasing backfill. 8m high pillar (w/h=2.5) with cohesive backfill on left non-cohesive backfill on right.

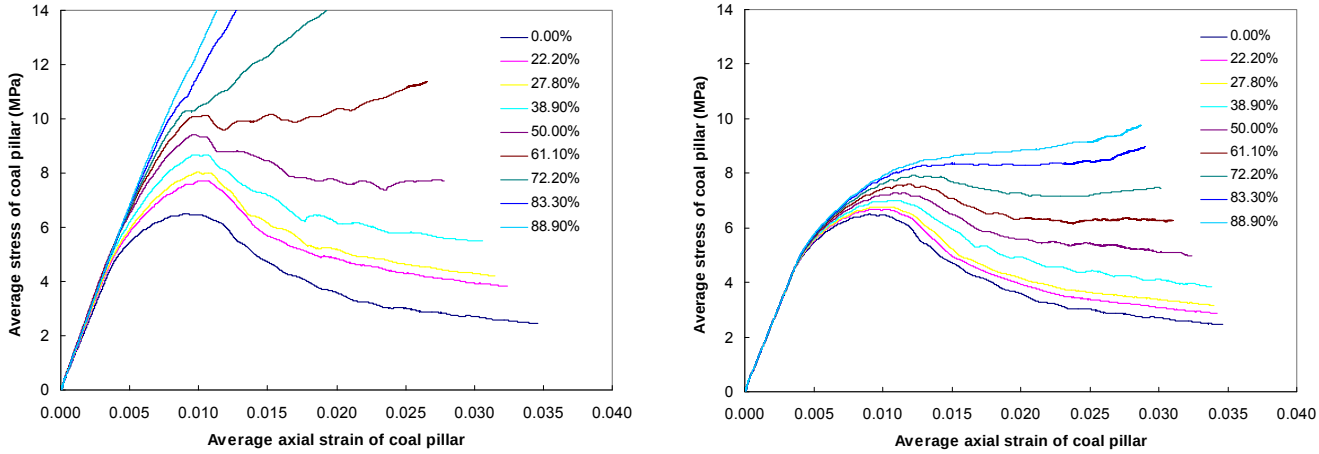

Figure A-43 Post peak pillar strength with increasing backfill. 9m high pillar (w/h=2.2) with cohesive backfill on left non-cohesive backfill on right.

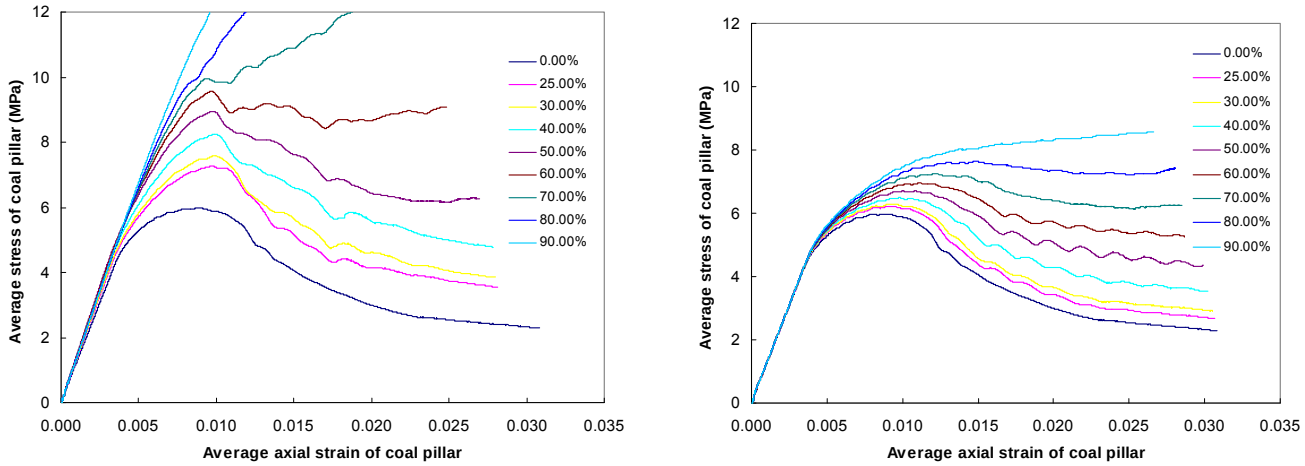

Figure A-44 Post peak pillar strength with increasing backfill. 10m high pillar (w/h=2.0) with cohesive backfill on left non-cohesive backfill on right.

The amount of backfill to achieve the transition between strain softening and hardening is presented in Table A-9 for all mining height. The values in this table are estimated from the stress-strain curve analysed to 3.5% of strain and are depended on the backfill increment which is in turn dependent on the ratio of mining height to the calibrated element size 0.5m.

Table A-9 Percentage of roadway backfill that leads to a transition from strain softening to hardening.

Pillar height	Non-cohesive backfill	0.5MPa Cohesive backfill	1.0MPa Cohesive backfill
5m	30.0%	20.0%	20.0%
6m	50.0%	41.7%	33.3%
7m	57.1%	50.0%	42.9%
8m	62.5%	62.5%	50.0%
9m	72.2%	72.2%	61.1%
10m	80.0%	80.0%	70.0%

The modelling results suggest that the average axial stress of coal pillar increases with compression until peak stress is reached. In the post-failure region, pillar stress is reduced as strain increases for all models without backfill. All the model results predict that there would be a change to strain hardening behaviour as percentage of backfill increases. For example, this transition point is 33.3% for 1.0 MPa cohesive backfill while 50% for non-cohesive backfill with 6m mining height as shown in Table A-9. It can also be seen from Table A-9 that tall pillars need more backfill than squat pillars to achieve the change from strain softening to hardening for either cohesive backfill or non-cohesive backfill.

A.5.5 Backfill for diamond shaped pillars

A 7m high diamond shaped pillar with 50 degree skew angle is analysed with increasing level of backfill in surrounding roadways. On the skewed angle the backfill is constrained with roller boundary conditions normal to the skewed angle to represent symmetry conditions and a 5m wide roadway.

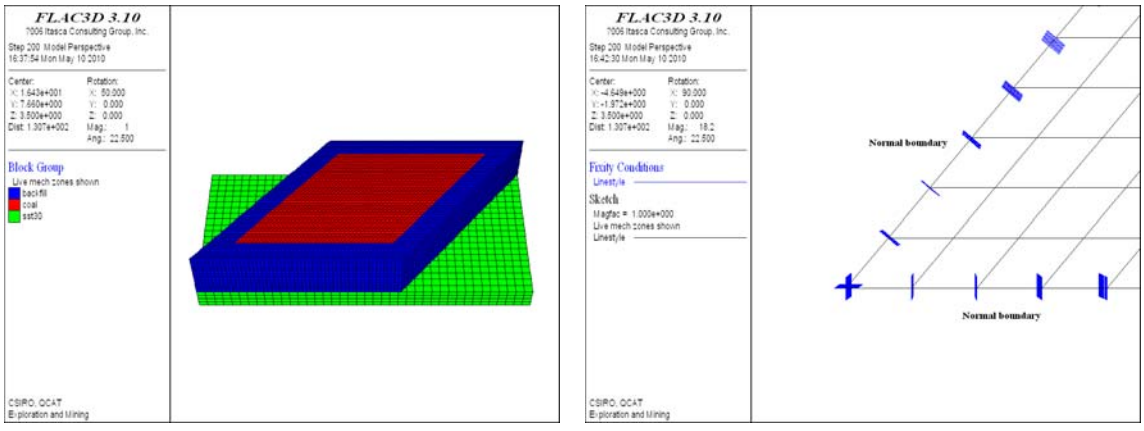

Figure A-45 Numerical model of diamond shaped pillar with backfill on left and boundary conditions on right

The predicted strength of a diamond shaped pillar and equivalent square pillar with increasing roadway backfill of both cohesive and non-cohesive models is presented in Figure A-46 and Figure A-47.

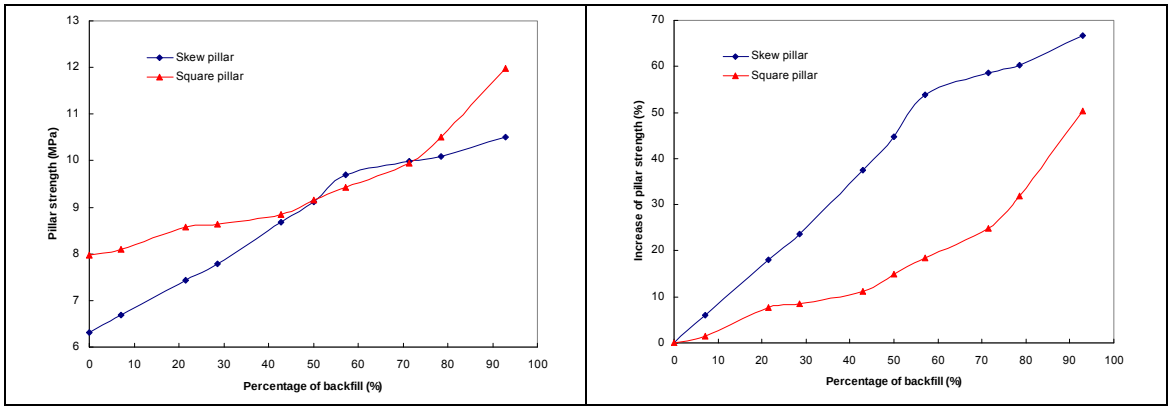

Figure A-46 Predicted pillar strength of diamond and square shaped pillars with increasing percentage of 1MPa cohesive backfill. On left is absolute strength and on right is percentage strength increase.

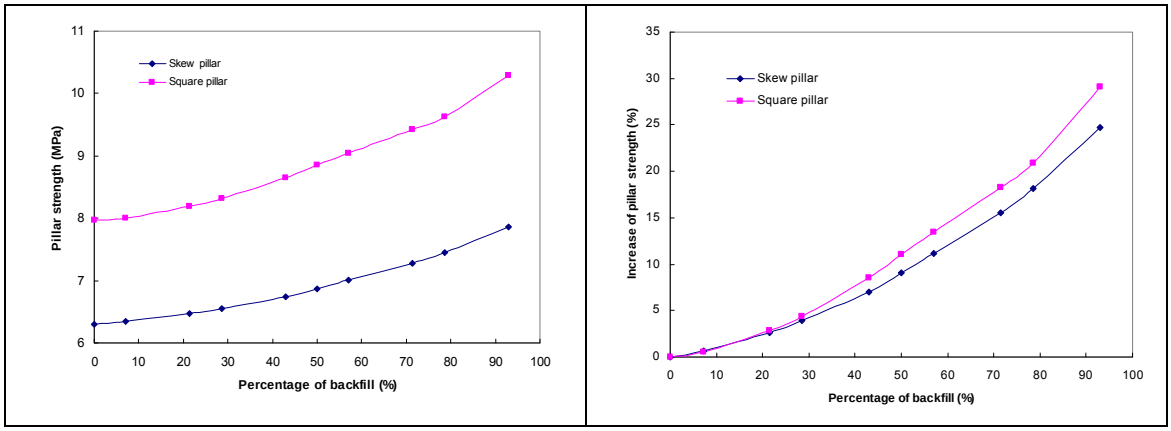

Figure A-47 Predicted pillar strength of diamond and square shaped pillars with increasing percentage of non-cohesive backfill. On left is absolute strength and on right is percentage strength increase.

A.5.6 Backfill placed after significant pillar yield

A pillar model with 90% non-cohesive backfill placed after yielding of a 7m high pillar is presented in Figure A-48. The percentage of strength increase is given in Table A-10. It is found that the pillar strength increase is lower if the pillar has undergone significant deformation before the placement of backfill. It is predicted that 90% backfill results in a strain-hardening pillar behaviour even if the pillar has previously yielded significantly.

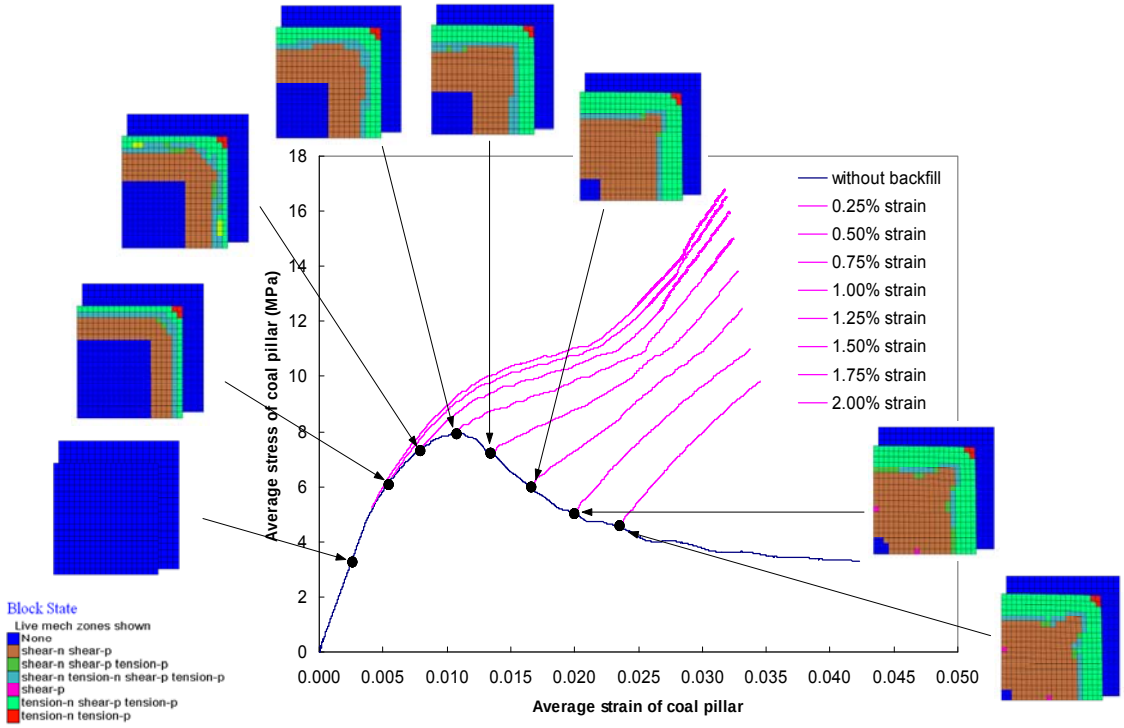

Figure A-48 Stress strain curves for backfill placed around the pre-strained pillar displaying state of pillar core upon placement of backfill.

Table A-10 Pillar strength increase with 90% non-cohesive backfill placed around a pre-strained 7m high square pillar of 20m width.

Percentage backfill (%)	Strain at placement of non-cohesive backfill (%)	Pillar strength (MPa)	Percentage increase in peak strength (%)	Percentage increase in post-peak strength at 3% strain (%)
0	0.00	7.953	0.00	/
90	0.00	10.290	29.39	/
90	0.25	9.156	15.13	/
90	0.50	8.965	12.72	/
90	0.75	8.526	7.20	/
90	1.00	7.945	/	260.06
90	1.25	7.951	/	226.08
90	1.50	7.951	/	189.17
90	1.75	7.951	/	156.29
90	2.00	7.951	/	111.34

A.6 3D MODEL OF DUNCAN ST FAILURE PANEL

A.6.1 Numerical model

A three dimensional model of 46 pillars in the Duncan St subsidence region has been analysed with over burden geology based on hole CP1 and a constant overburden depth of 124m, Figure A-49, Figure A-50 and Figure A-51. Uniform mining heights of 6m and 9m have been analysed.

Selection of the pillars to be analysed is based on visual inspection of the panel layout and includes pillars bounded by unmined coal to the west, the waterline barrier pillar to the east, larger pillars to the south and a panel of slightly larger pillars of different orientation to the north.

One row of pillars in the middle of this panel trending from north-west to south-east are of smaller dimension than the average and of diamond shape with acute internal angle of approximately 50degrees. Being in the approximate middle of the panel close to full tributary area load will be mobilised on this row of pillars and therefore it is believed pillars in this row initiated the 2008 subsidence event.

The Duncan Street numerical model has the following objectives.

- Estimation of pillar stresses and FoS for comparison with empirical formula;
- Comparison of backfill response at panel scale with previous single pillar studies;
- Estimation of surface subsidence at given percentage roadway fill;
- Estimation of extent of abutment stresses due to panel failure;

A.6.2 Observations from Duncan Street numerical model

- At 6m mining height, the minimum pillar FoS for these 46 pillars is calculated to be 1.31 using Pressure Arch theory and UNSW strength formula, panel failure is not predicted with this mining height by the model. At 9m mining height the minimum FoS is calculated as 0.99 and panel failure is predicted to occur.
- The probability of pillar failure for associated FoS calculated by the UNSW pillar strength formula, Eq.(2) is given in Galvin 2006 in Table A-11. The relationship was developed for square pillars using the Australian pillar database and tributary area theory, and hence theoretically speaking may not directly apply to this study. However, it can be taken as a general guide.
- From Table A-11 it is seen that there is a 1 in 20 probability of instability at 6m mining height, and a 1 in 2 probability at 9m mining height. Numerical modelling is however a deterministic approach, and it always predicts failure if the FoS is less than 1.0 and stability if FoS > 1.0 since no variation in geotechnical properties or conditions is used.

- Although our numerical models predict no pillar failure at 6m and panel failure at 9m, in reality there remains approximately a 1 in 20 chance of failure at 6m mining height. If one pillar was to fail, load transferred to adjacent pillars would reduce the FoS of these adjacent pillars and could lead to the pillar failure and subsidence as observed at 2008 event region.

Table A-11 Factor of safety failure probabilities for UNSW pillar strength formula. (after Galvin 2006)

Safety Factor	Probability of pillar failure
0.87	8 / 10
1.00	5 / 10
1.22	1 / 10
1.30	5 / 100
1.38	2 / 100
1.44	1 / 100
1.63	1 / 1000
1.79	1 / 10000
1.95	1 / 100000
2.11	1 / 1000000

- Based on the numerical results obtained using two mining heights, the pillar and overburden failure is consistent with analytical predictions from Pressure Arch theory and UNSW pillar strength calculation.
- Surface subsidence predicted from the numerical model with a mining height of 9m is 1.96m. While this value is in approximate agreement with monitoring data (1.4m-1.5m), the model was not sufficiently calibrated, since the real mining height in the region is uncertain, to be able to confidently predict final subsidence, strains and tilts at the site.
- With 1MPa cohesive backfill at a roadway fill ratio of 83%, the predicted strength increase is 70%. With non-cohesive backfill at the same fill ratio, the strength increase is 20%. These values are in agreement with the results for single pillars.
- The numerically predicted surface subsidence with 83% roadway fill is 0.22m. Maximum predicted tilt in east-west direction is 7mm/m and in north-south direction is 5mm/m. Analytical formula [Holla & Barclay 2000] predict maximum tilt of 5.3mm/m for this amount of subsidence.
- Isolated cohesive backfill surrounding pillars of low *w/h* ratio is predicted to be effective in confining the pillar and increasing peak pillar strength and panel stability. Isolated non-cohesive backfill without barriers could not be analysed in this numerical model as backfill ‘flows’ and numerical stability could not be achieved.

- Stress transfer in the immediate roof sandstone unit (above the coal roof) is predicted to extend approximately 80m beyond the limits of the collapsed panel. This is in reasonable agreement with theoretical studies.

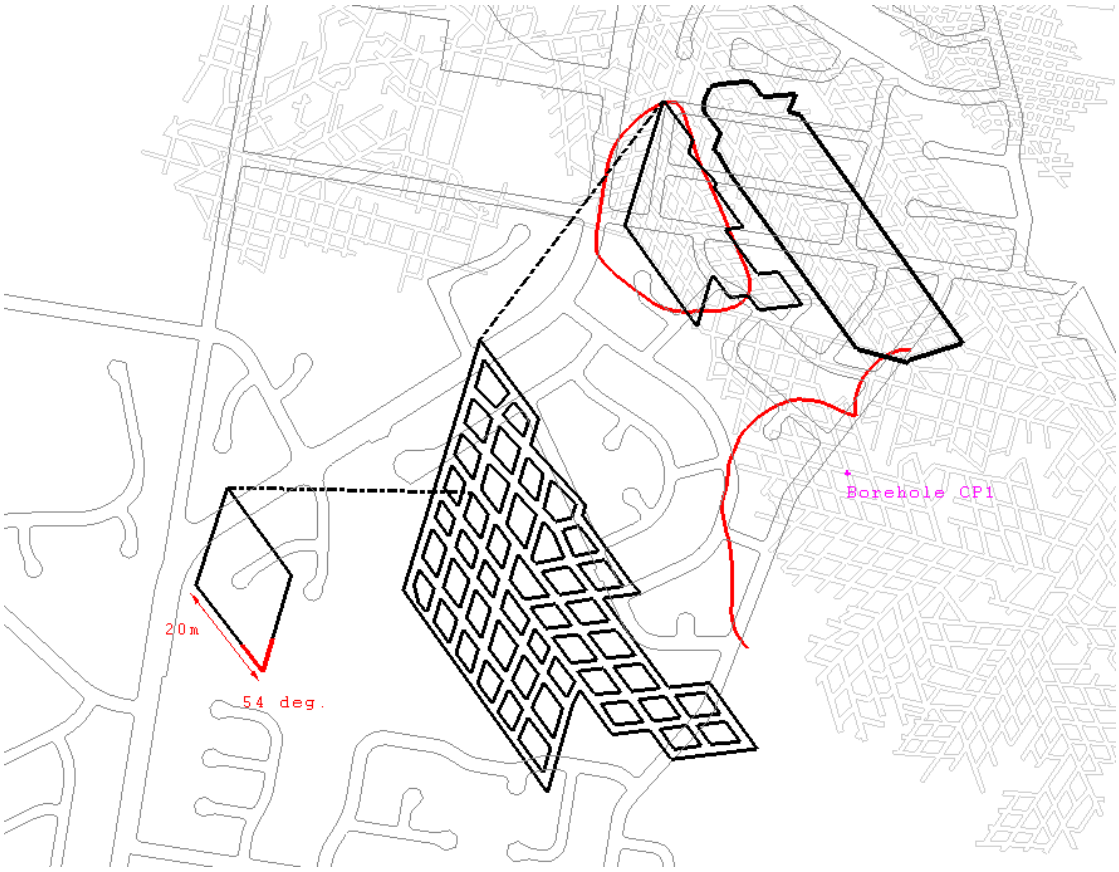

Figure A-49 Duncan St modelled panel with outline of adjacent modelled panel, location of representative open hole CP1, file named “Appendix B2 open hole logs” located in directory “Collingwood Park Subsidence / 2B Collingwood Park Mine Subsidence Reports / 1988 Events” and mine subsidence limit contour.

A.6.3 Model properties

Overburden geology is based on borehole CP1, the most complete interpreted available hole drilled in 1988 by Queensland Department of Mines, Figure A-50. To include this in the numerical model lithological units had to be coalesced into major units of sandstone (SS), siltstone (SL), mudstone (MS), weathered units and coal, Figure A-51.

Rock properties for the overburden were determined from a 2D parametric study whereby the UCS of all units was scaled to achieve pillar and overburden failure at 8m mining height, Table A-12 and Table A-13.

Unit top depth	thickness	unit	thickness	thickness scaled	thickness in model
0.00	12.00	weathering	12.00	10.46	10.00
12.00	7.00	SS	7.00	6.10	6.00
19.00	6.00	MS	6.00	5.23	5.00
25.00	11.00	SS	13.00	11.33	11.00
36.00	2.00	SS		0.00	
38.00	1.00	SL	10.00	8.71	9.00
39.00	1.00	MS		0.00	
40.00	5.00	MS/ SS		0.00	
45.00	1.00	SL / SS		0.00	
46.00	1.00	SL / MS		0.00	
47.00	1.00	MS		0.00	
48.00	1.00	SS	4.00	3.49	4.00
49.00	3.00	SS		0.00	
52.00	3.00	SL	7.00	6.10	6.00
55.00	1.00	MS		0.00	
56.00	3.00	MS		0.00	
59.00	4.00	SS	5.00	4.36	4.00
63.00	1.00	SS		0.00	
64.00	4.00	SL / SS	9.00	7.84	8.00
68.00	1.00	SL / MS		0.00	
69.00	1.00	SL		0.00	
70.00	2.00	SL / MS		0.00	
72.00	1.00	SS / SL		0.00	
73.00	2.00	SS	10.00	8.71	9.00
75.00	2.00	SL		0.00	
77.00	2.00	SS / SL		0.00	
79.00	2.00	SS		0.00	
81.00	1.00	SL		0.00	
82.00	1.00	SS		0.00	
83.00	2.00	SL	43.50	37.90	38.00
85.00	2.00	SL		0.00	
87.00	1.00	SS		0.00	
88.00	1.00	COAL		0.00	
89.00	2.00	SL / MS		0.00	
91.00	1.00	MS		0.00	
92.00	1.00	SS		0.00	
93.00	1.00	SL / MS		0.00	
94.00	3.00	SL / MS / SS		0.00	
97.00	1.00	MS		0.00	
98.00	1.00	SL / MS		0.00	
99.00	4.00	SL / SS		0.00	
103.00	2.00	SS / MS		0.00	
105.00	1.00	SL / MS		0.00	
106.00	2.00	SL / MS / SS		0.00	
108.00	1.00	MS		0.00	
109.00	4.00	SL / MS		0.00	
113.00	4.00	SL / SS		0.00	
117.00	1.00	SS / MS		0.00	
118.00	3.00	SL		0.00	
121.00	4.00	SL / SS		0.00	

125.00	1.50	SL / MS		0.00	
126.50	4.50	SS	8.50	7.41	7.50
131.00	4.00	SS		0.00	
135.00	1.00	MS / SL	9.60	8.37	5.00
136.00	2.00	SS / SL			
138.00	1.00	SS			
139.00	2.00	SS / SL			
141.00	3.60	SL / MS			
144.60	4.70	COAL	MINING SEAM		6.00
149.30		FLOOR			

Figure A-50 Inferred geology from representative borelog CP1 used in numerical model.

Unit	Depth floor below surface	Num elements	Unit #	Unit name in model
surface	0			
weathering	10	3	16	weather
SS	16	2	15	ss6
MS	21	2	14	ms2
SS	32	4	13	ss5
SL	41	3	12	sl3
SS	45	1	11	ss4
MS	51	2	10	ms1
SS	55	1	9	ss3
SL	63	3	8	sl2
SS	72	3	7	ss2
SL	105.5	11	6	sl1
SS	113	4	5	ss1
SEAMR	118	3	4	seamr
SEAM	124	3	3	seam
FLOOR1	134	3	2	floor2
FLOOR2	250	10	1	floor1

Figure A-51 Coalesced units for numerical model based on hole CP1.

Insitu stress is unknown at the site so a horizontal to vertical stress gradient of 1.5 has been assumed. Given that the extensive workings were undertaken 20 to 30 years before the 2008 event horizontal stresses in the mining seam would be considerably disturbed from the pre-mining conditions.

Table A-12 Rock properties for softening mohr coloumb material. Softening rates of coal friction angle is 6 degrees over 2% plastic strain and total loss of cohesion over 2.4% plastic strain in coal and over 1% in other rocks. Determined from pillar studies.

	E (GPa)	nu	Bulk (GPa)	Shear (GPa)	UCS (MPa)	UCS scaled	Phi	Dilation angle	Coh (MPa)	Tensile Strength (MPa)
SS	7.5	0.2	4.167	3.125	50	12.5	40	2	2.91	1.25
SL	4	0.25	2.667	1.600	30	7.5	35	2	1.95	0.75
MS	3	0.25	2.000	1.200	15	3.75	32	2	1.04	0.375
Weathering	1	0.25	0.667	0.400	8	2	32	2	0.55	0.2
COAL	1.1	0.3	0.917	0.423	12	3	36	6	0.76	0.03
FLOOR1	4	0.25	2.667	1.600	30	7.5	38	2	1.83	0.75
FLOOR2	4	0.25	2.667	1.600	30	7.5	38	2	1.83	0.75

Table A-13 Ubiquitous joint properties. Softening rate of ubiquitous joints total loss of cohesion over 1% plastic strain. Determined from 2D overburden studies.

	Cohesion (MPa)	Ubiq joint cohesion (MPa)	Tensile Strength (MPa)	Ubiq joint tensile strength (MPa)	Ubiq joint friction
SS	2.91	0.0029144	1.25	0.000125	15
SL	1.95	0.0019521	0.75	0.000075	15
MS	1.04	0.0010393	0.375	0.0000375	15
Weathering	0.55	0.0005543	0.2	0.00002	15
COAL	0.76		0.03		
FLOOR1	1.83	-	0.75	-	-
FLOOR2	1.83		0.75		-

A.6.4 Results from 3D Duncan St model

Factor of Safety estimated at 6m and 9m mining heights

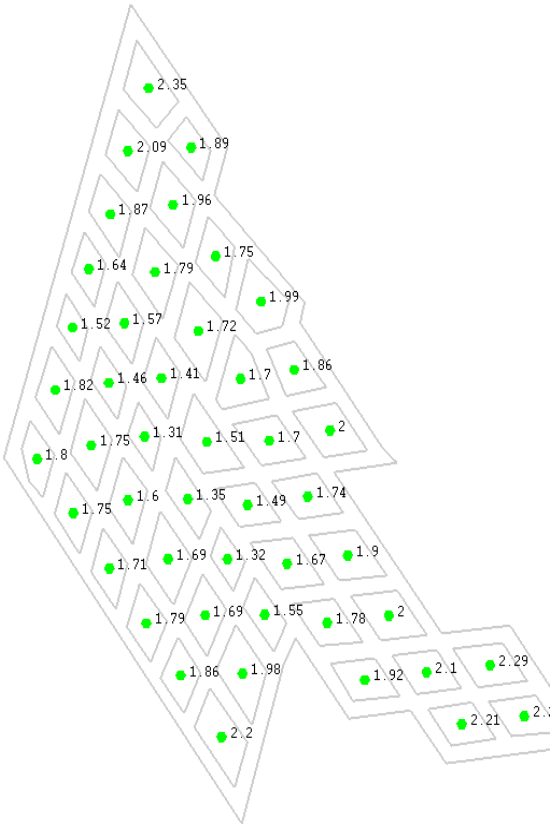

Figure A-52 Pillar FoS calculated for 6m mining height by analytical method with strength by eq(3) and pillar stress by pressure arch theory. Minimum value is 1.31 suggesting a 5 in 100 probability of failure however not sufficient to fail in the numerical model (that requires FoS < 1.0).

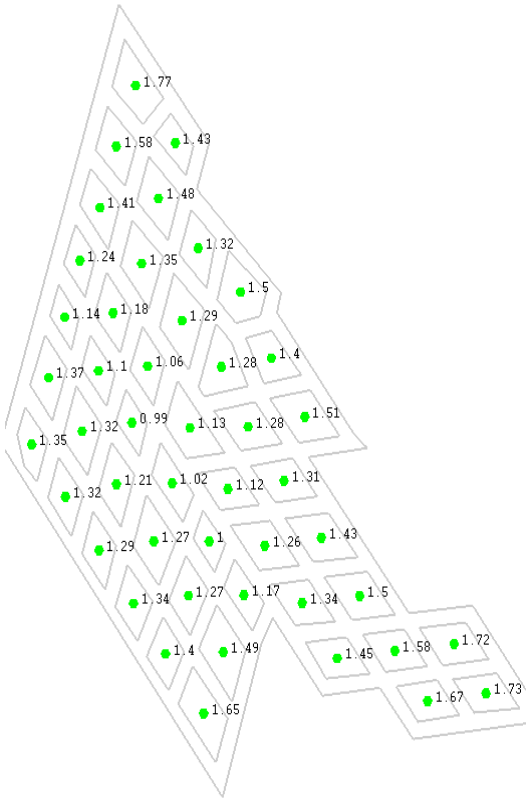

Figure A-53 Pillar FoS calculated analytically for 9m mining height (eq(3) and PA theory). Minimum value is 0.99 suggesting a probability of failure of 5 in 10 although in the numerical model failure should occur.

Yield on plane for 6m and 9m mining heights

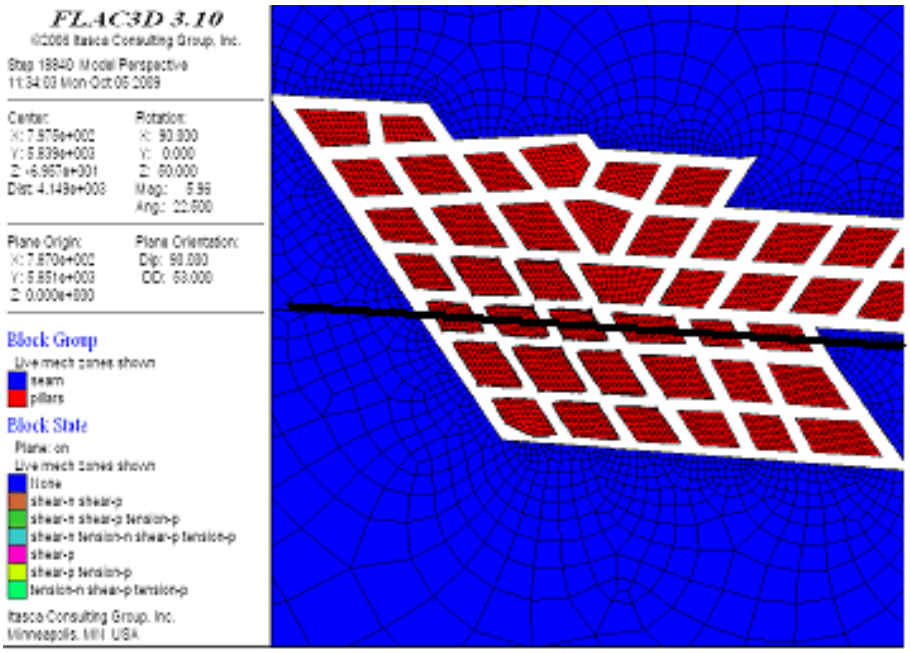

Figure A-54 Location of section plane used for section view in following figures.

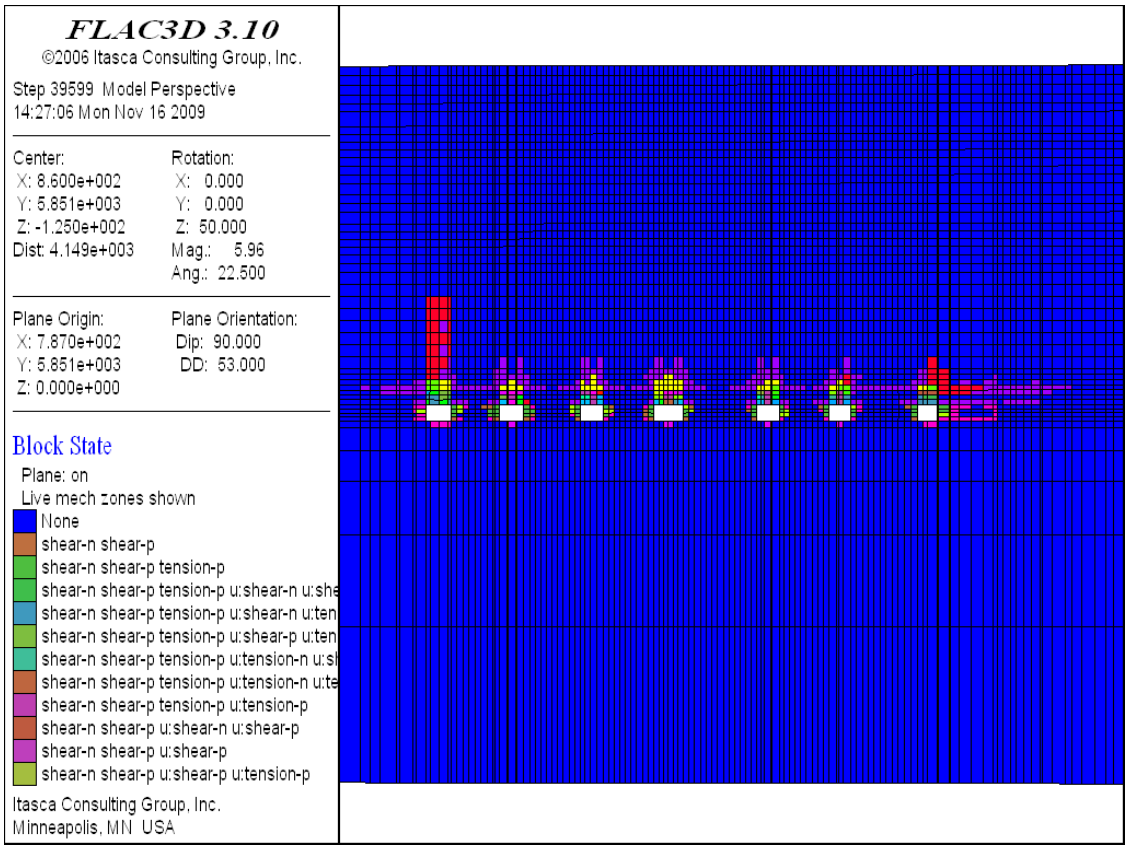

Figure A-55 Yield on section plane for 6m mining height. No significant damage or displacement observed.

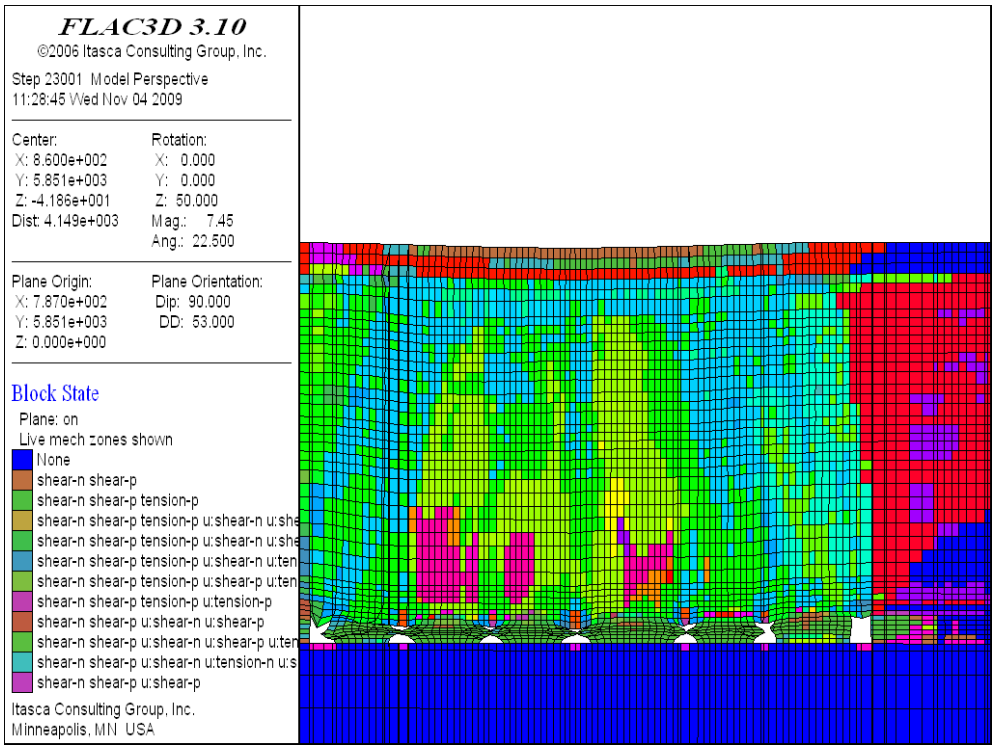

Figure A-56 Yield on section plane for 9m mining height, no backfill.

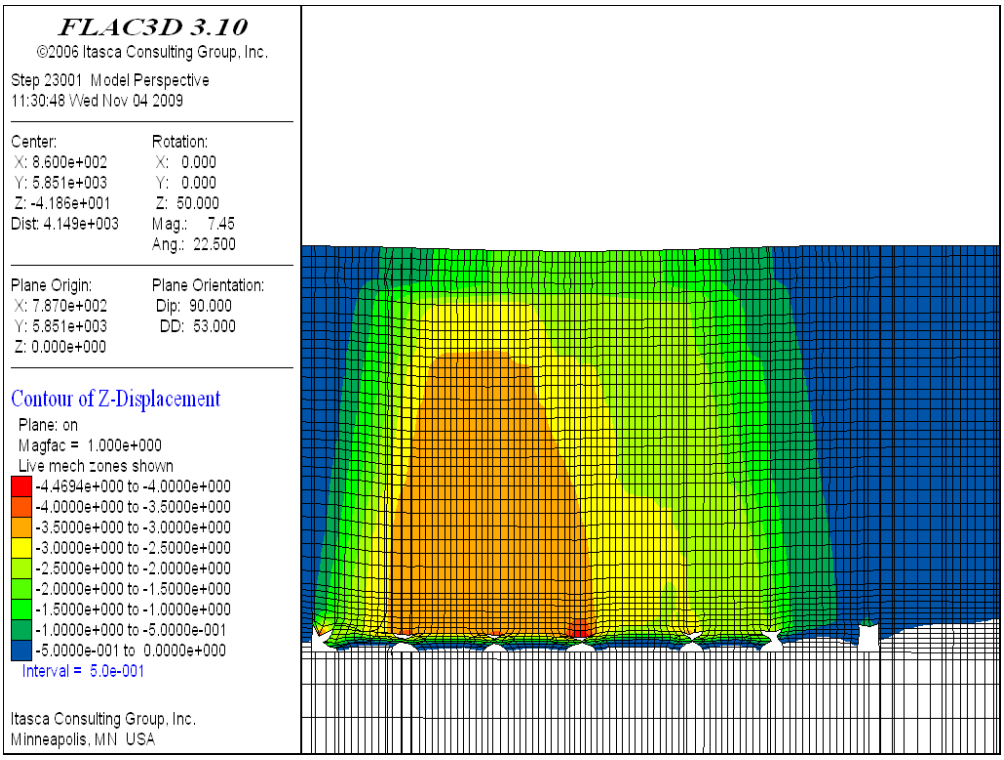

Figure A-57 Displacement on section plane for 9m mining height, no backfill. Maximum displacement is approximately 1.5m at surface.

Results on horizontal plane at mid-pillar height

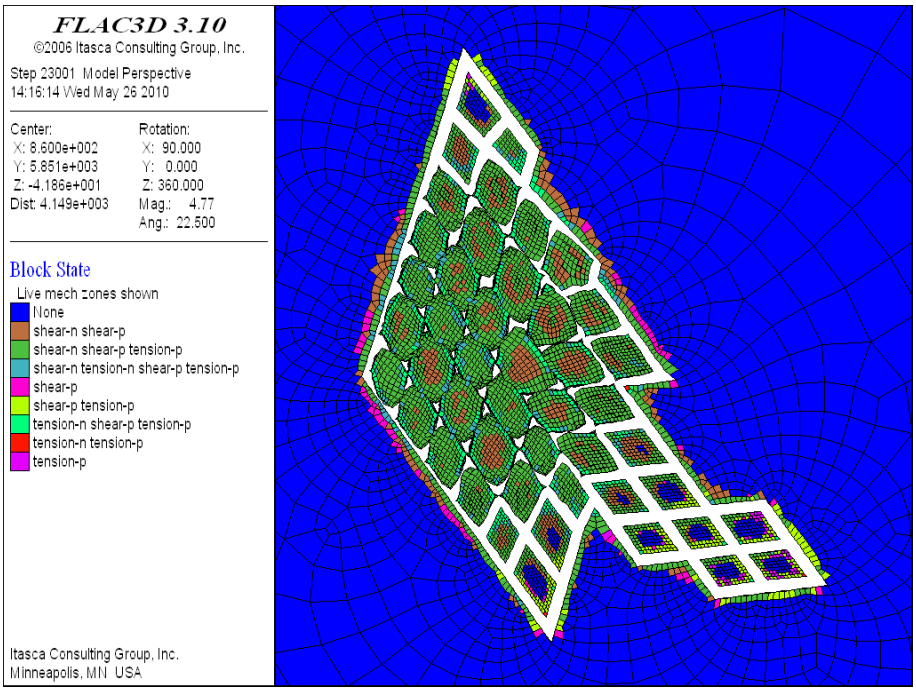

Figure A-58 Yield at mid-pillar height, 9m mining height. Blue elements evident in some pillars indicating pillar core remains intact.

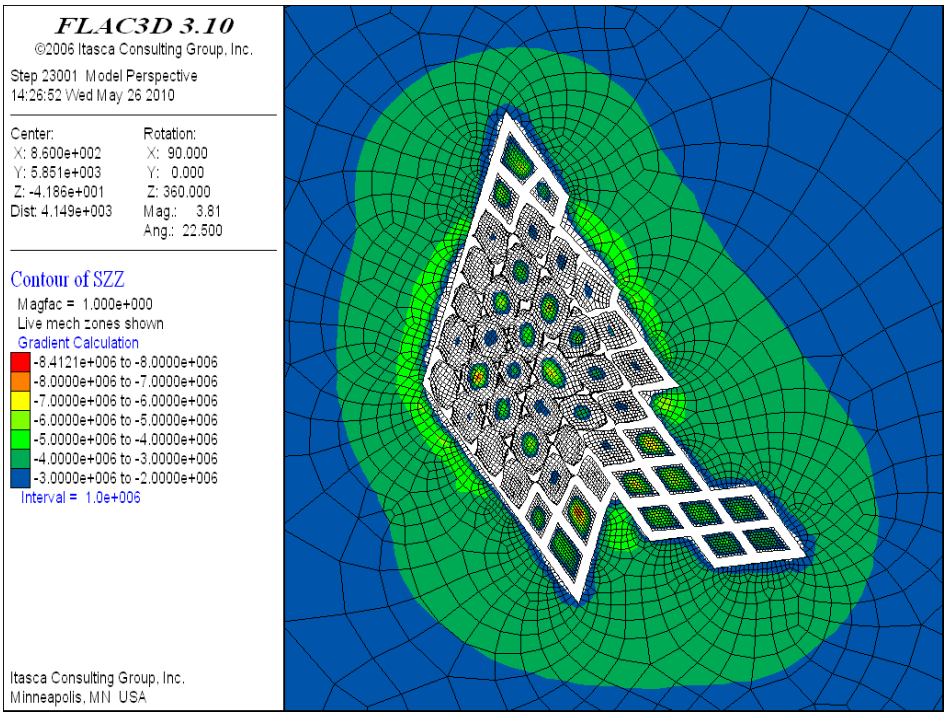

Figure A-59 Predicted vertical stress at mid pillar height, 9m mining height. Insitu stress is 3.0MPa. Unyielded pillars and pillars hardening after yield are transferring vertical load while yielded pillars carry little load. Extent of abutment stress increase is approximately 80m.

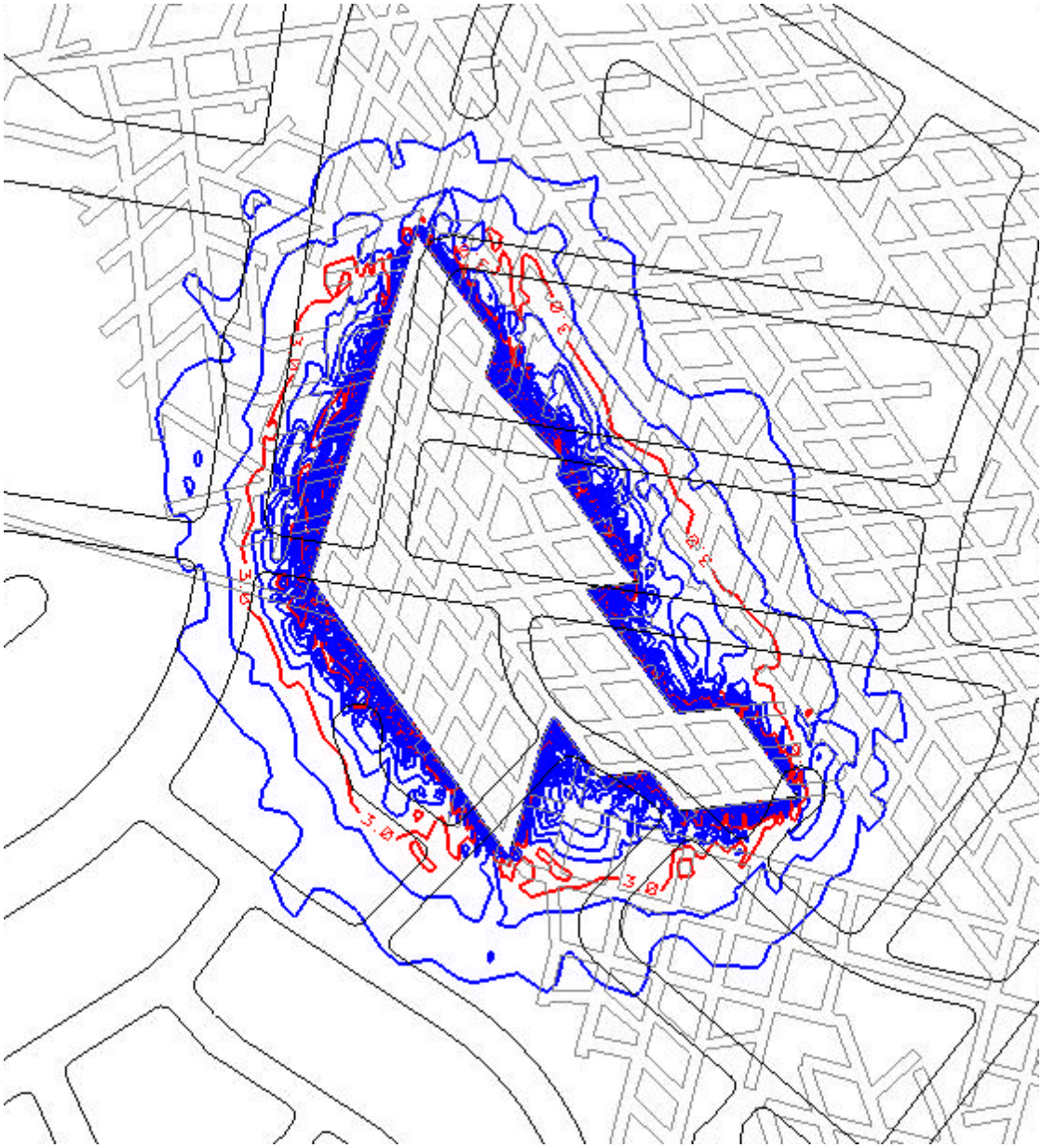

Figure A-60 Roof vertical stress predicted by numerical model with 9m mining height. Contour increments are 0.1MPa. Base vertical stress is approximately 2.7MPa. Abutment stress influence distance is approximately 80m.

Results on surface after panel failure at 9m mining height

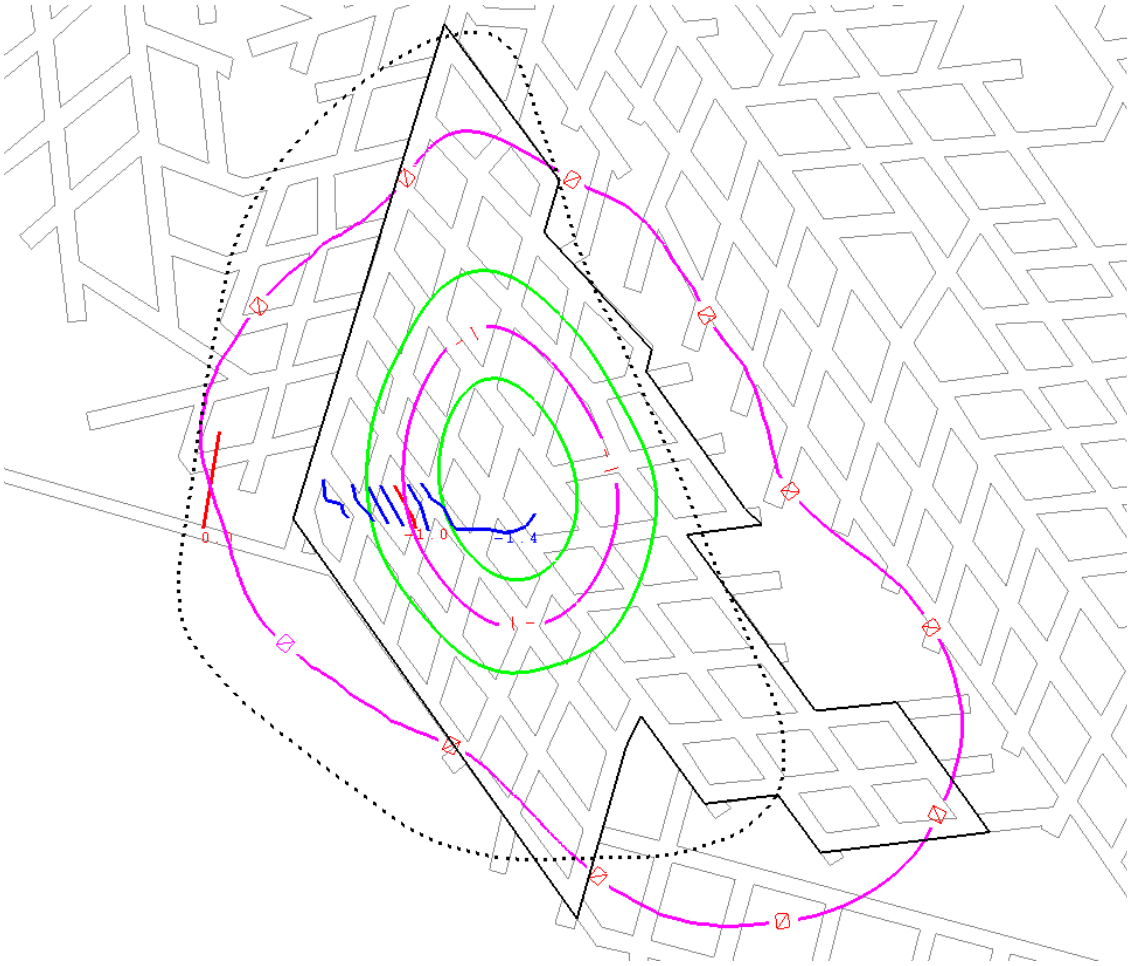

Figure A-61 Surface subsidence, as predicted with numerical model with 9m mining height and total subsidence along Duncan St to McLaughlin St as monitored to October 09. Maximum surface subsidence predicted as 1.96m. Outline of numerical modelling pillars and dotted contour of observed subsidence limit.

A.6.5 Duncan St model – backfill effectiveness

The Duncan St 3D model has been analysed with full and targeted 1MPa cohesive and non-cohesive backfill placed in roadways. Roadway fill of 66% is analysed for the 1MPa cohesive mixture and 83% roadway fill for the non-cohesive mix.

Results are presented in the following figures and figure captions.

Factor of Safety increase from cohesive backfill

Analysis of the Duncan St model with 9m mining height is undertaken to estimate the FoS increase from backfill. By increasing gravity in increments the backfill strength improvement is quantified. With 83% roadway fill of 1MPa cohesive backfill the overburden and pillar tops (ie region of pillar above height of backfill) fails with gravity of 17m/s^2 suggesting the pillars with FoS of approximately 1.0 has increased FoS to 1.7 by backfilling adjacent roadways.

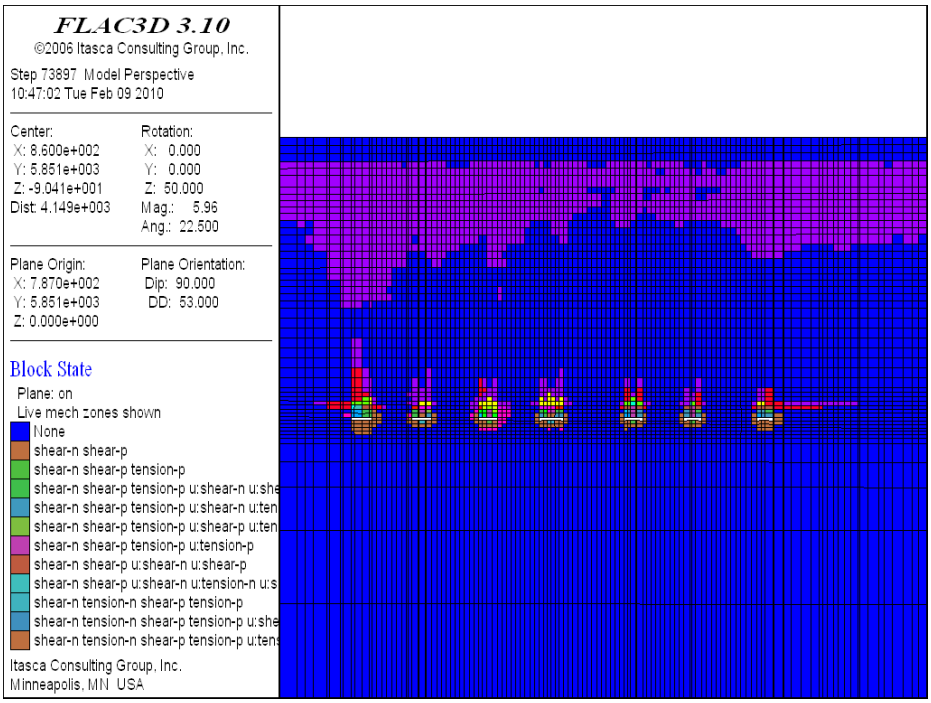

Figure A-62 Gravity of 1.6g with 83% 1MPa cohesive backfill showing no significant yield.

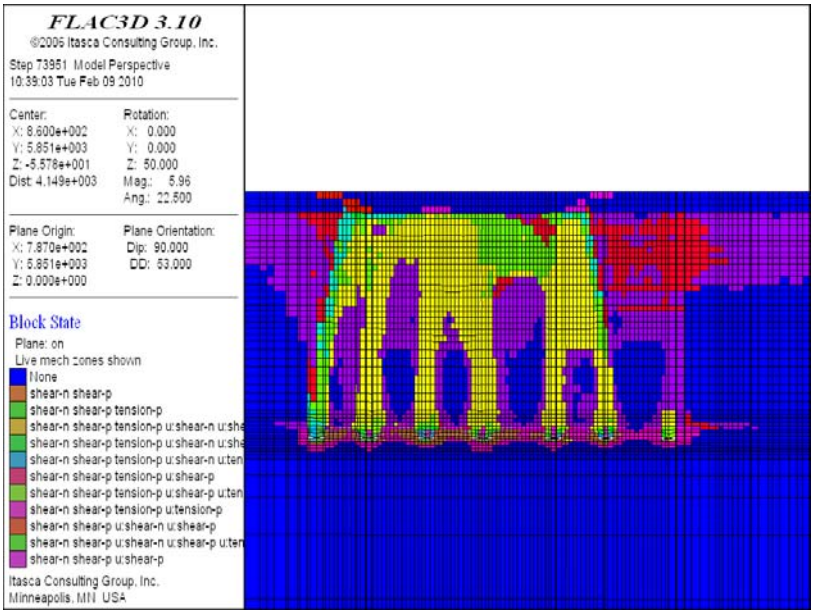

Figure A-63 Gravity of 1.7g with 83% 1MPa cohesive backfill predicting failure of pillar tops and overburden and collapse of roadway void space.

FoS increase with non-cohesive backfill

With non-cohesive backfill pillars yielded due to lack of confinement upon initial placement of backfill in roadways but overburden remain stable and void space above backfill remained open. Overburden remained stable at gravity increase to 11m/s^2, Figure A-64 but collapsed at gravity increase of 12m/s^2, Figure A-65.

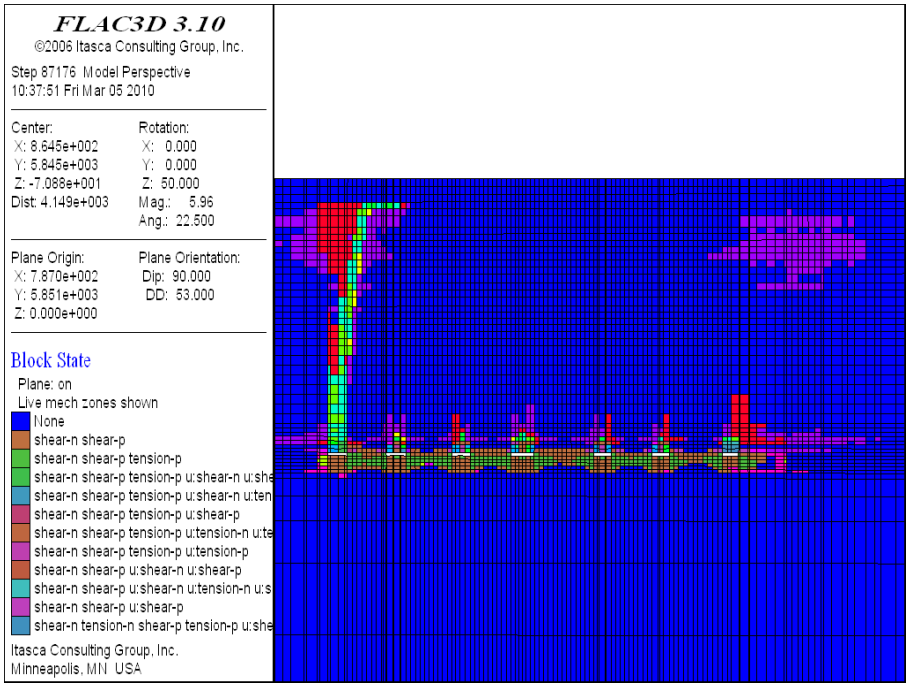

Figure A-64 Gravity of 1.1g with 83% non-cohesive backfill predicting pillar yield but overburden stability

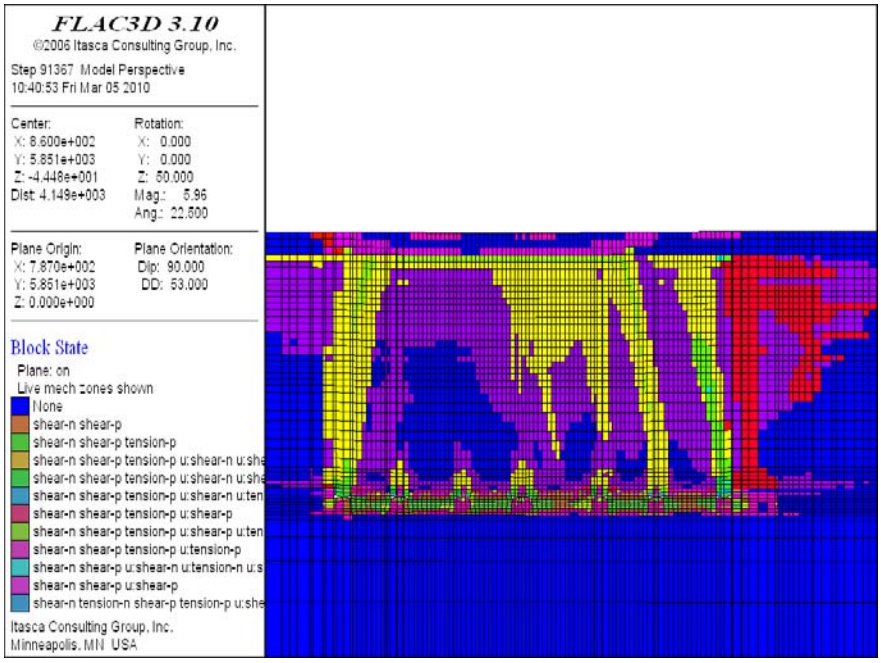

Figure A-65 Gravity of 1.2g with 83% non-cohesive backfill predicting failure of pillars and overburden and collapse of roadway void space. Maximum surface subsidence is 0.55m which includes the compressive effect of the 1.2g gravity increase.

Placement of targeted backfill

A model is analysed with cohesive backfill totally surrounding two pillars with low predicted FoS. The two pillars are predicted to have a FoS of 0.99 and 1.00 left to right viewed from above at a 9m mining height. Backfill extends to an extent of 5m to 10m from the pillar and is 6m high in the roadways. Gravity increase to 1.2g required to fail panel suggesting panel strength increase is approximately 20% from targeted backfill. Predicted surface subsidence 1.25m (excessive mesh deformation stops analysis, equilibrated stage may have higher surface subsidence).

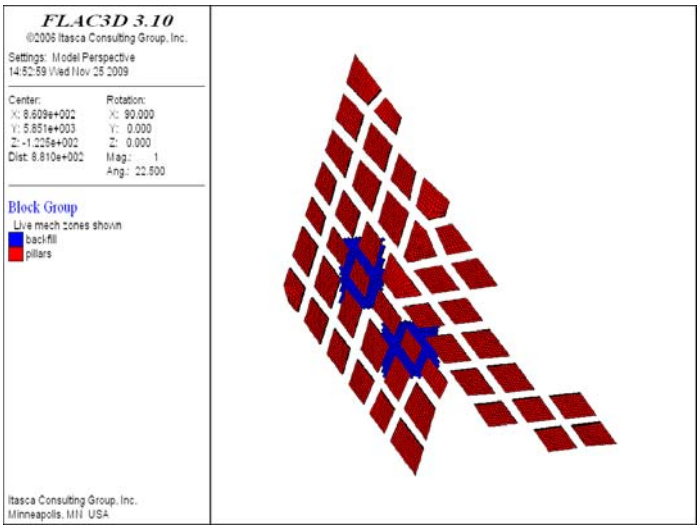

Figure A-66 Duncan St model with 66% roadway fill of 1MPa cohesive backfill surrounding two pillars with low FoS at 9m mining height.

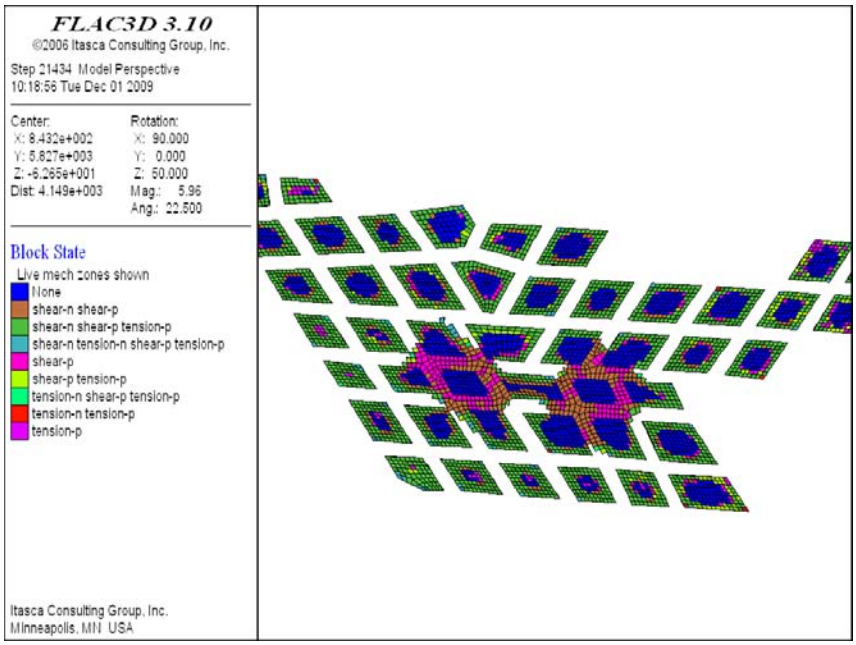

Figure A-67 Predicted yield at mid pillar height of 9m pillars with 66% roadway fill of 1MPa cohesive backfill. Note intact core (blue) for targeted pillars.

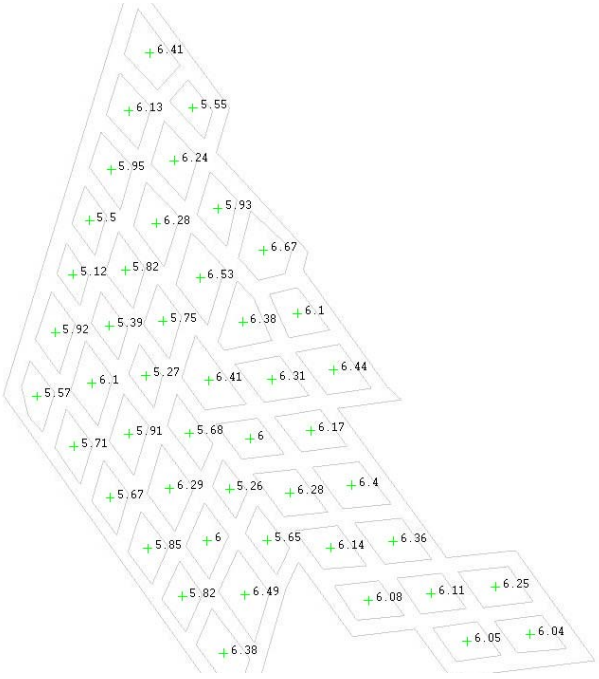

Figure A-68 Pillar strength at 9m mining height. Strength WITHOUT BACKFILL of northern focus pillar selected for targeted backfill is 5.27MPa and southern focus pillar is 5.26MPa.

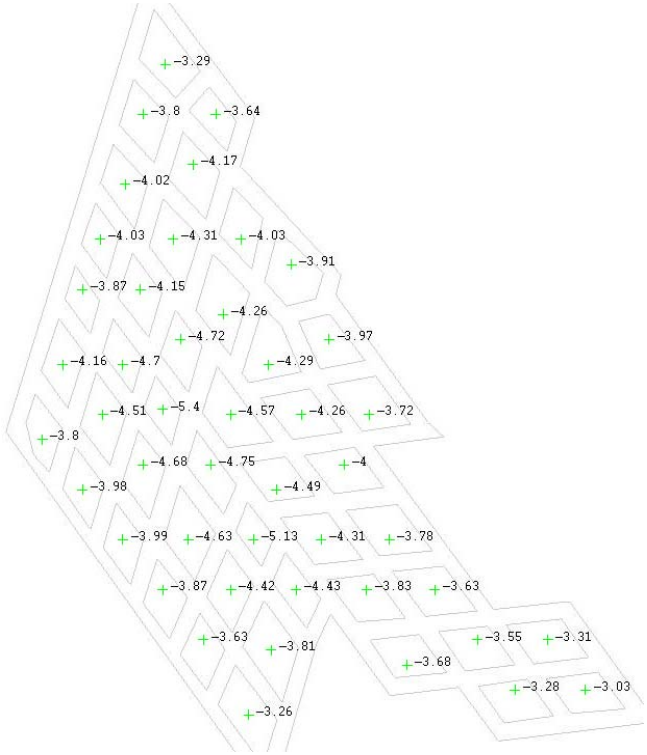

Figure A-69 Vertical stress in pillars targeted for partial backfill placement. Stress calculated at equilibrium of elasto-plastic analysis WITHOUT BACKFILL. Stress in northern focus pillar is 5.4MPa and in southern focus pillar is 5.13. FoS of NFP=5.27/5.4 = 0.975, FoS of SFP=5.26/5.13 = 1.025

Non-cohesive backfill in targeted placement study

A model with targeted placement of non-cohesive backfill was attempted but could not be satisfactorily converged since backfill 'flows' and inter-penetrates elements resulting in numerical instabilities.

Forcing pillars to fail to examine resultant subsidence

To examine the extent of surface subsidence if backfilled pillars fail, the numerical model with 9m mining height and 83% roadway fill of 1MPa cohesive backfill is analysed with a 90% reduction in coal pillar strength properties.

With 9m mining height and 83% roadway fill of cohesive backfill void space remaining is 1.5m and the numerical model predicts failure of pillars and overburden results in approximately 0.2m surface subsidence.

Figure A-70 Surface subsidence predicted by numerical model when pillars forced to fail with 83% roadway fill. Contour interval is 0.1m with maximum subsidence predicted as 0.22m.

Figure A-71 Surface strain in east-west direction when pillars forced to fail resulting 0.22m surface subsidence. Maximum strain is 5mm/m and contour interval is 1mm/m.

Figure A-72 Surface strain in north-south direction when pillars forced to fail resulting 0.22m surface subsidence. Maximum strain is 3mm/m and contour interval is 1mm/m.

Figure A-73 Tilt in east-west direction. Units are mm/m and intervals are 1mm/m, maximum tilt is 7mm/m.

Figure A-74 Tilt in north-south direction. Units are mm/m and intervals are 1mm/m, maximum tilt is 5mm/m.

To highlight the need for adequate fill, the model with 66% roadway fill is analysed with the pillars forced to fail with a 50% reduction in pillar strength. Void space over the backfill in the roadways is 3.0m. Modelling predicts maximum surface subsidence of 0.68m.

Figure A-75 Surface subsidence when pillars forced to fail with 66% roadway fill. Roadway void space is 3.0m with the model predicting 0.68m surface subsidence. Contour interval is 0.1m.

A.6.6 Numerical model of adjacent high risk area

Numerical model and panel stability

A numerical model of the region adjacent to Duncan St incorporating 76 pillars is analysed at 9m mining height. Overburden strata, strengths and depth-of-cover is consistent with Duncan St model.

The main objective of this model is to estimate the strength difference between the two mining panels west and east of the Waterline fault. Given uniform mining height and depth-of-cover the strength difference will be due to the pillar configuration and boundary conditions.

At 9m mining height the model is predicted to be essentially stable although 9 pillars are predicted to be fully yielded at mid-pillar height.

With gravity increase of 10% the model remains stable. At 20% increase in gravity the model is predicted to fail with significant overburden yield.

It is concluded therefore that the panel to the east of Waterline fault is 20% stronger than the panel to the west.

Figure A-76 Location of numerical model #2 together with surface subsidence contours from 1988 and 2008 events and seam level eastern boundary of failure predicted from 3D seismic.

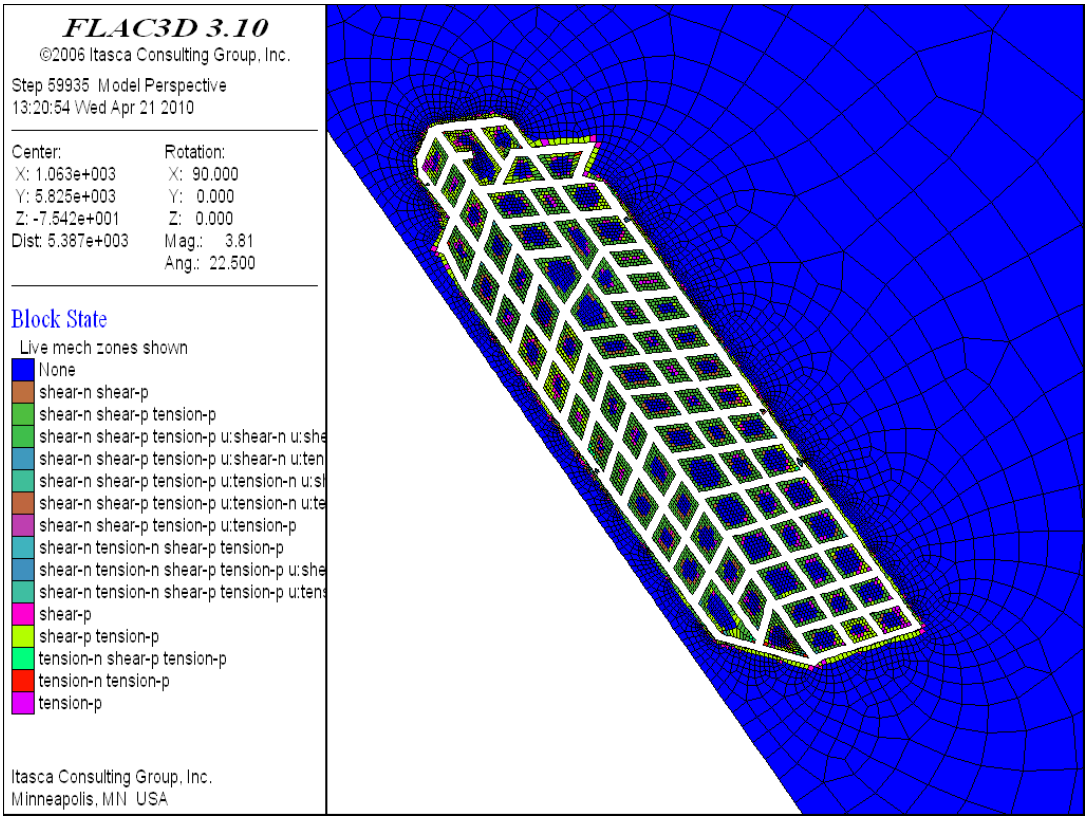

Figure A-77 Yield on section at mid-height for 9m mining height.

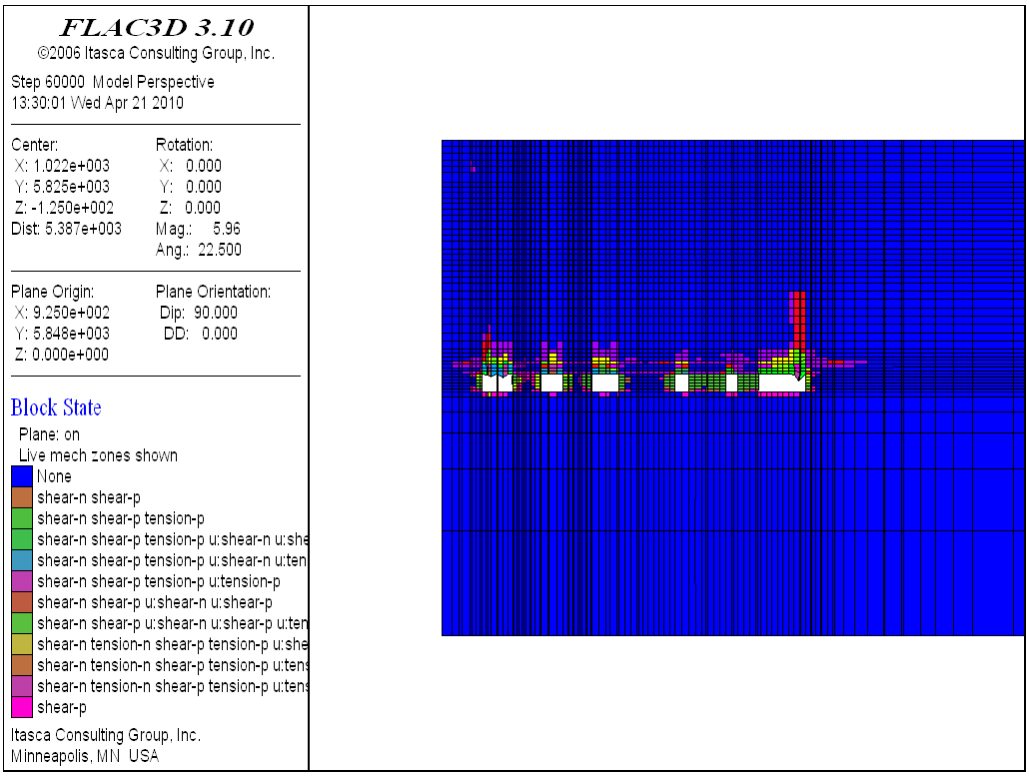

Figure A-78 Rockmass yield on vertical section trending east-west at mid-point of model. Note overburden is largly intact with no extensive collapse.

Figure A-79 Pillars predicted to have failed from Numerical model #2 with surface subsidence contours and inferred eastern limit of failed zone at seam level.

By a 20% increase in gravity the model is forced to fail resulting in predicted 1.3m surface subsidence that includes increased overburden compression from increased gravitational component. Excessive deformation and numerical instability stopped the model, true surface deformation may be higher.

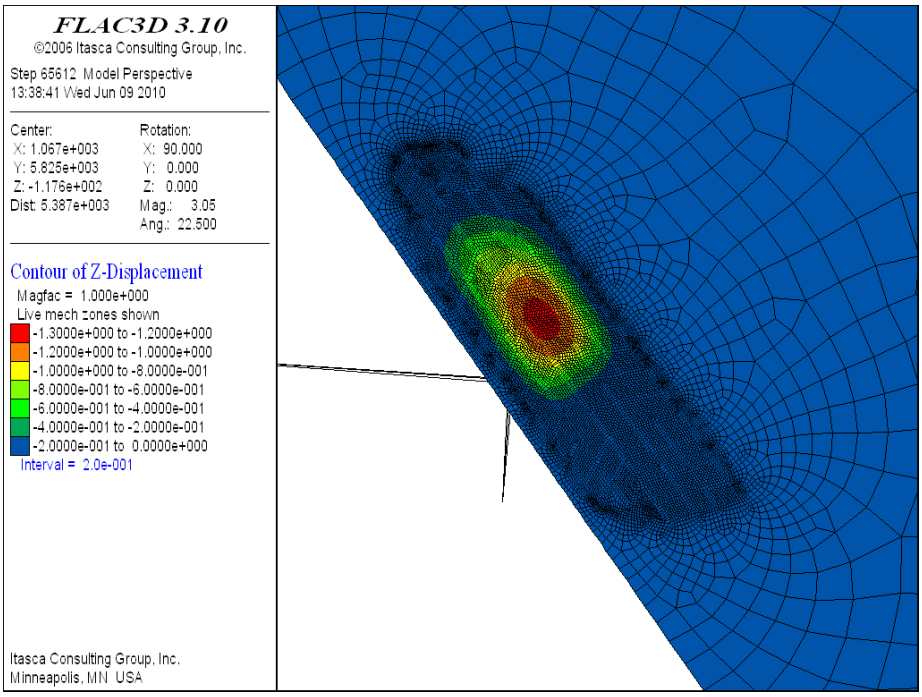

Figure A-80 Adjacent model with 9m mining height. Predicted surface subsidence after 20% increase in gravity. Model predicts 1.3m surface subsidence.

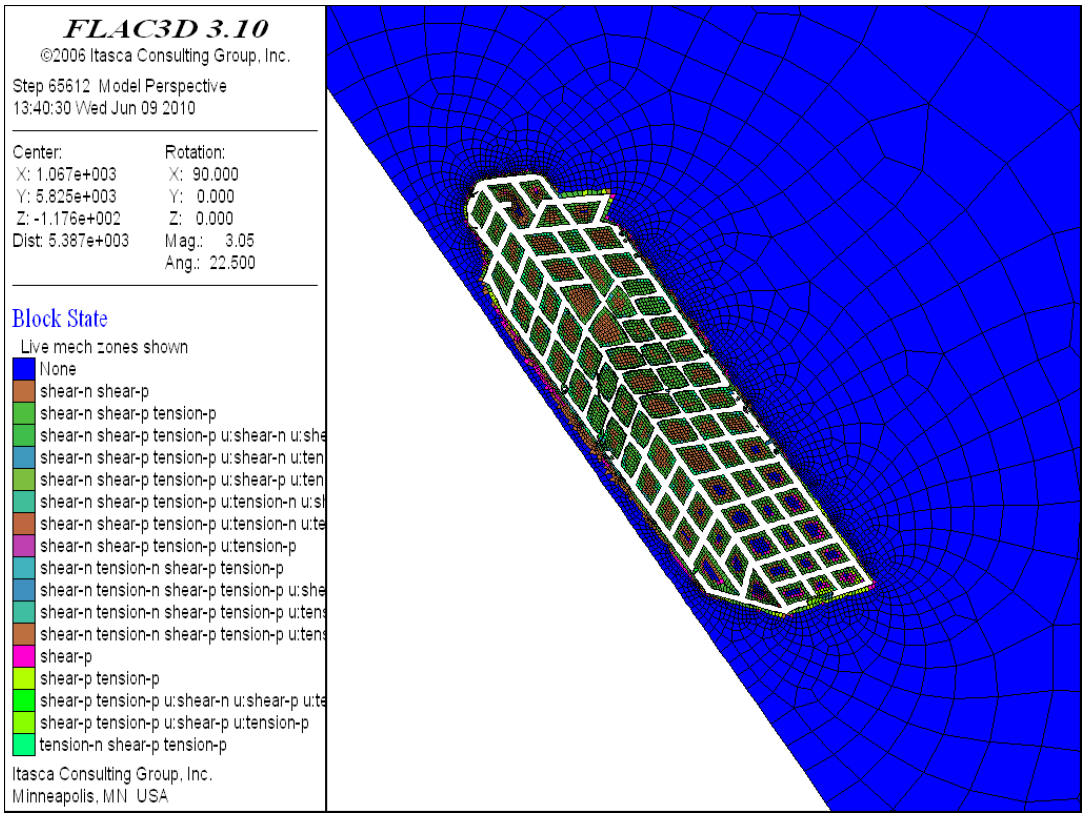

Figure A-81 Adjacent model with 9m mining height and 20% gravity increase. Predicted failure at mid-pillar height. Note intact core in southern pillars which appear stronger from unmined adjacent coal and larger general pillar size.

A.7 CONCLUSIONS

A.7.1 Current knowledge on coal pillars behaviour

- The strength based factor-of-safety approach is well established in coal pillar design. Factors of safety for coal pillars required to provide medium to long term stability should be greater than 1.6 [Galvin, 2006, Hill, 2005].
- Coal pillar strength has been the subject of rigorous research since at least the 1960's and the Salamon & Munro formula has been applied in the design of over a million coal pillars in South Africa alone [Mark, 1999, Salamon, 1998]. Strength formula derivations from the UNSW are established in Australia.
- Coal pillar load calculation traditionally relies on tributary area theory which is a conservative approach suitable for pillar *design.*
- Tributary area conditions are ***NOT*** satisfied at Collingwood Park; pillars are irregular in size and shape, there is large areas of unmined coal and the seam has significant dip.
- This last point is important as analytical methods hold the only hope of evaluating *every* pillar at Westfalen No. 3 Colliery. The numerical model of Duncan St analyses 46 pillars and requires significant computational resources, the entire Colliery has in excess of 700 pillars and cannot be analysed by the same methods in its entirety by current computer codes in a reasonable time frame.
- Likewise it is not satisfactory to draw conclusions on panel stability from limited analysis of representative groupings of pillars because of the variability in size, shape, mining height and cover depth over the mining area.
- To overcome the limitations of tributary area theory for the back-analysis of an irregular pillar layout, a novel approach for calculating loads based on pressure arch theory has been developed subjected to international peer review and published in the International Journal of Rock Mechanics and Mining Sciences. In summary, each pillar is individually examined and the pillar area, circumference and centroid are calculated. At the pillar centroid the cover depth and mining height are determined. An influence zone based on a circular area with radius defined by the depth-dependent load transfer distance. Within this area, the local extraction ratio is calculated. This approach has found to satisfactorily account for pillars of arbitrary shape in irregular layout with variable cover depth.
- This allows a FoS to be determined for the over 700 pillars of Westfalen No. 3 with reasonable computer resources.

A.7.2 Typical pillar strength effects

Width to height ratio

- Pillars at Westfalen No. 3 have typical effective width from 20m to 50m. While mining height is uncertain it is believed to range from 6m to 10m. With these dimensions pillar *w/h* ratio ranges from 2.0 to 8.3.
- At the lower limit of *w/h*=2.0 geological influences will start to determine pillar strength [Galvin 2006]. From *w/h* in the range > 2.0 to 4.0 the formula of Salamon and Munro or UNSW extensions could be expected to estimate pillar strength with the squat pillar version of these formula applicable for *w/h>4.0* [Galvin 2006, Salamon 1998, Galvin 1999].
- The squat pillar extensions were developed since the standard formulas were found to *underestimate* pillar strength at *w/h*>4. At Westfalen No. 3 colliery, although there are a number of pillars of *w/h*>4 many of these are irregular in shape often long and relatively narrow (30m – 40m). Given this and the need to automate the assessment of *every* pillar the squat pillar strength formula *is not* utilised. This approach is conservative.

Pillar shape effects

- Many pillars at Westfalen No. 3 are skewed of *diamond* shape with acute internal angle from 50 to 90 degrees. Hydraulic radius simile accounts for pillar shape by an effective width defined by *4A/C* while the UNSW has a parrellopid formula that for pillars of equal side length results in an effective width equivalent to this.
- In a study of pillar shapes common to Westfalen No. 3 colliery the hydraulic radius analogy for estimation of effective width is found adequate with errors less than 6% for considered sizes and shapes.

Post peak strength

- Numerical studies and the work of Das in Indian coal fields highlights the changing post peak behaviour with increasing width to height ratio's. It has been determined that when *w/h* exceeds approximately 5, pillars start to harden post peak. When *w/h*<3 pillars display limited, if any, post peak strength.
- The significance of this effect will be in the manner that pillars shed load to adjacent pillars. In an array of pillars of similar dimensions, pillars with a low *w/h* ratio could be expected to shed load in a sudden, more catastrophic manner than those that harden post peak. Such sudden pillar failure is referred in the literature as catastrophic, cascading or rolling pillar failure and has been responsible for damaging wind blasts and significant loss of life over the years.
- In an irregular pillar layout such as Westfalen No. 3 with variable *w/h* ratio, significant barrier pillars and regions of unmined coal, sudden multiple panel collapse would be expected to be less likely.
- The analytical approach developed for assessing pillar load accounts for load shed from a failed pillars to pillars within the zone of influence of that pillar.

Specific details of this approach are discussed in the hazard map and risk assessment chapter of this report.

Backfill effect

- Numerical studies on a cohesive and non-cohesive backfill suggest that pillar strength is increased with increasing height of fill. Studies suggest a 1MPa cohesive backfill may increase pillar strength by approximately 10% at 40% roadway fill for *w/h=3.3* and 18% at 40% roadway fill at *w/h=2.2.* At 80% roadway fill pillar strength increases are predicted to exceed 50%. Percentage strength increases are predicted to be greater with lower *w/h* ratio's.
- Studies of a non-cohesive backfill suggest at 80% roadway fill pillar strength increases are approximately 25%.
- With both backfill types pillar strength is predicted to increases dramatically above 80% roadway fill and pillars are predicted to exhibit post-peak hardening behaviour.

  For example, in the Duncan St area a pillar of effective width 20m, will have a FoS of approximately 1.18 at mining height of 10m without backfill. A 50% strength increase from 1MPa cohesive backfill at 80% roadway fill will raise the FoS to approximately 1.77 and reduce the probability of instability from approximately 1 in 10 to less than 1 in 1000.

  With 80% roadway fill of a non-cohesive backfill, the same Duncan St pillar FoS will increase to approximately 1.47 and the probability of instability reduce to less than 1 in 100.
- Backfill is likely to reduce the rate of time dependent pillar strength degradation by reducing pillar spalling due to the erosive effects over time of high stress and exposure of the pillar surface to the atmosphere.
- In addition, backfill is likely to benefit pillar stability by limiting the void available to the roof to fall into. Roof falls, particularly at roadway intersections may be present. By reducing the roadway volume, backfill will eventually support the roof when the bulking effect of roof falls fills the remaining roadway voids space. Beyond this summary, time dependent issues of backfill have not been considered.

% roadway fill	Non-cohesive backfill (7m mining height, width 20m) % strength increase	0.5 MPa cohesive backfill (7m mining height, width 20m) % strength increase	1.0 MPa cohesive backfill (7m mining height, width 20m) % strength increase
60	13.5	38.8	43.7
70	18.3	43.2	59.7
80	20.8	47.4	69.8
90	29.1	57.2	95.7

A.7.3 Duncan St numerical model

- In the Duncan St subsidence region approximately 46 pillars are surrounded by unmined coal to the west, a large pillar containing the Waterline fault to the east and larger pillars to the south and north.
- At 6m mining height pillar minimum FoS for these 46 pillars is calculated at 1.31 with Pressure Arch theory and UNSW strength formula. At 9m mining height minimum FoS is calculated as 0.99.
- Pillar probability of failure for FoS calculated by the UNSW eq(2) is given in [Galvin 2006] as:

Table A-14 Factor of safety failure probabilities for UNSW pillar strength formula. (after Galvin 2006)

Safety Factor	Probability of pillar failure
0.87	8 / 10
1.00	5 / 10
1.22	1 / 10
1.3	5 / 100
1.38	2 / 100
1.44	1 / 100
1.63	1 / 1000
1.79	1 / 10000
1.95	1 / 100000
2.11	1 / 1000000

- From Table A-14 at 6m mining height there is a 1 in 20 probability of instability and at 9m a 1 in 2 probability. The variability in the database of failed and unfailed pillars from which eq (1) to eq (3) are derived is responsible for these probabilities. Our numerical model should always predict failure if the FoS is less than 1.0 and always predict stability with FoS > 1.0 since no such variability in geotechnical properties or conditions is used.
- While our numerical model predicts no pillar failure at 6m and pillar failure at 9m, in reality there remains approximately a 1 in 20 chance of failure at 6m mining height. If one pillar was to fail, load transferred to adjacent pillars would reduce these adjacent pillars FoS and may well lead to the pillar failure and resultant subsidence observed at Duncan St.
- Based on the numerical results obtained using two mining heights, the pillar and overburden failure is in line with analytical predictions from Pressure Arch theory and UNSW pillar strength calculation.

- Surface subsidence predicted from the 9m mining height numerical model is 1.96m. While this value is in general agreement with monitoring data, the model is not sufficiently calibrated, since the real mining height in the region is unknown, to be able to confidently predict final subsidence, strains and tilts.
- With 1MPa cohesive backfill at a fill ratio of 83%, the predicted strength increase is 70%. With non-cohesive backfill at the same fill ratio, the strength increase is 20%, these values are in agreement with single pillar studies.
- Abutment stresses in the immediate roof sandstone unit (above the coal roof) are predicted to extend approximately 80m beyond the limits of the model. This is in reasonable agreement with twice the load transfer distance of 64m (at 124m depth-of-cover) used to define a pillars zone of influence (the ZI also includes half pillar width, ie 74m for 20m pillar)

A.7.4 Numerical model of adjacent region

- A numerical model of the region immediately to the east of the Duncan St failure region is constructed with 76 pillars.
- At 9m mining height the model predicts failure of 9 pillars but no significant overburden failure. The model remains stable in general.
- With a 20% increase in gravity the model is predicted to fail.
- Numerical modelling results suggest the region to the east of the Waterline barrier pillar is stronger by approximately 20% than the subsided region to the west of the barrier pillar.
- Predicted surface subsidence (including compressive effects from gravity increase) is 1.3m all though numerical instabilities halt the model and true surface subsidence is likely to be higher.
- Inspection of yield at mid-pillar height suggests the southern pillars in the model have intact core when pillars in the middle of the region are failed in their entire volume. In reality the southern region of this panel have greater depth-of-cover, therefore higher pillar stresses and thus lower FoS in these southern pillars.